Morphological and molecular characterization of three new *Azadinium* species (Amphidomataceae, Dinophyceae) from the Irminger Sea

Urban Tillmann[1*], Marc Gottschling[2], Elisabeth Nézan[3], Bernd Krock[1], Gwenaël Bilien[3]

[1] Alfred Wegener Institute, Am Handelshafen 12, D-27570 Bremerhaven, Germany

[2] Department Biologie, Systematische Botanik und Mykologie, GeoBio-Center, Ludwig-Maximilians-Universität München, Menzinger Str. 67, D-80638 München, Germany

[3] IFREMER, Station de Biologie Marine, Place de la Croix, BP 40537, 29185 CONCARNEAU Cedex, France

Running title: Three new species of *Azadinium*

*Corresponding author: Urban Tillmann, Alfred Wegener Institute for Polar and Marine Research, Am Handelshafen 12, D-27570 Bremerhaven, Germany

Email address: Urban.Tillmann@awi.de

Phone +49 471 4831 1470; Fax +49 471 4831 1425

Abstract

Some species of planktonic *Azadinium* produce azaspiracids (AZAs), a group of lipophilic phycotoxins causing human poisoning after mussel consumption. We describe three new species from the North Atlantic, all of which shared the same Kofoidean plate pattern characteristic for *Azadinium*: Po, cp, X, 4´, 3a, 6´´, 6C, 5S, 6´´´, 2´´´´. *Azadinium trinitatum* sp. nov. was mainly characterized by the presence of an antapical spine and by the position of the ventral pore at the left distal end of the pore plate in a cavity of plate 1´. *Azadinium cuneatum* sp. nov. had a conspicuously formed first apical plate, which was asymmetrically elongated and tapered on its left lateral side with a ventral pore located at the tip of this elongated 1´ plate. *Azadinium concinnum* sp. nov. was of particular small size (< 10 µm) and characterized by an anteriorly elongated anterior sulcal plate and by large and symmetric precingular plates. The ventral pore was located inside the apical pore plate on the cells' right lateral side. Molecular phylogenetics as inferred from concatenated SSU, ITS, and LSU sequence data supported the distinctiveness of the three new species. None of the new species produced any known AZAs in measurable amounts.

Key words: *Azadinium*, azaspiracids, Irminger Sea, Iceland, new species

Introduction

A large number of marine biotoxins produced by micro-algae are known to accumulate in shellfish making it harmful for human consumption. Intoxications have been categorized based on diagnostic symptoms as Paralytic, Amnesic, Diarrhetic, and Neurotoxic Shellfish Poisoning (PSP, ASP, DSP, NSP). As a fifth category, Azaspiracid Shellfish Poisoning (AZP) was recently coined to account for a toxic syndrome associated with the consumption of animals contaminated with azaspiracid toxins. The history of azaspiracids (AZAs) extends back to November 1995, when a harvest of blue mussels cultivated in Killary Harbour (Ireland) was implicated in the poisoning of at least eight people in the Netherlands. Three years later, the causative toxin was isolated from mussels, identified, structurally defined and named azaspiracid according to its chemical characteristics (Satake et al. 1998). The AZA-producing organism, however, remained unknown until the isolation and identification of *Azadinium spinosum* Elbrächter et Tillmann from the North Sea (Tillmann et al. 2009) as a new species in a newly erected genus.

Considering the short interval since the first identification of *Azadinium*, the knowledge about its diversity has rapidly increased. The currently encountered seven species are the type species *A. spinosum* (Tillmann et al. 2009) and further *A. obesum* Tillmann et Elbrächter (Tillmann et al. 2010), *A. poporum* Tillmann et Elbrächter (Tillmann et al. 2011), *A. polongum* Tillmann (Tillmann et al. 2012b), *A. caudatum* (Halldal) Nézan et Chomérat [(Nézan et al. 2012); occurring in two distinct varieties: *A. caudatum* var. *margalefii* (Rampi) Nézan et Chomérat and *A. caudatum* var. *caudatum*], *A. dexteroporum* Percopo et Zingone (Percopo et al. 2013), and *A. dalianense* Z.Luo, H.Gu et Tillmann (Luo et al. 2013). Moreover, a close relative was identified with the description of *Amphidoma languida* Tillmann, Salas et Elbrächter, and *Azadinium* and *Amphidoma* were subsequently placed in the family Amphidomataceae (Tillmann et al. 2012a).

Cells of *Amphidoma* and *Azadinium* are generally small and rather inconspicuous in light microscopy. Determination of diagnostic morphological characteristics, such as presence/absence of an antapical spine and distinct pyrenoid(s), or the location of a ventral pore, requires electron microscopy or tedious high resolution light microscopy (Tillmann et al. 2009, 2010, 2012, 2012b). Reliable identification of fixed cells of *Azadinium* from field samples is thus problematic and is further challenged by similar size and shape in comparison to a number of small species of *Heterocapsa* F.Stein. However, there is a need to unambiguously identify and quantify the toxigenic source organisms of AZAs and to distinguish these from their non-toxigenic relatives. This task is challenging because AZA-producing and non-toxigenic species are known to co-exist in the same water mass (Tillmann et al. 2010, 2011, 2012b).

Multiple strains of the type species *A. spinosum*, collected at different localities, consistently produce AZA-1, AZA-2, and AZA-33 (an AZA with the molecular mass of 715; Tillmann et al. 2012b). Other species have initially been described as non-toxigenic, as none of the known AZAs have been identified (Tillmann et al. 2010, 2011). However, the recent detection of four new AZAs in species such as *A. languida* and *A. poporum* indicates that species diversity within the Amphidomataceae is also reflected by high chemical diversity (Krock et al. 2012). Molecular probes for the first three described species (*A. spinosum*, *A. obesum*, *A. poporum*) are now available (Toebe et al. 2013) and are in the stage of being tested in field application (Tillmann et al. 2014a).

It cannot be excluded, or it is even to be expected, that there are more yet undescribed species of the Amphidomataceae. These may either include a yet not recorded primary source of AZAs, or might yield false-positive (if non-toxigenic) signals with the molecular probes already designed for toxigenic *A. spinosum* and *A. poporum*. It is therefore important to gain more information on the diversity of species present in the Amphidomataceae, on their molecular signatures, and on their geographical distribution. Both the widespread records of

AZA toxins (Braña Magdalena et al. 2003; James et al. 2002; López-Rivera et al. 2009; Taleb et al. 2006; Yao et al. 2010) and the increasing number of records of species of *Azadinium* (Akselman and Negri 2012; Gu et al. 2013b; Hernández-Becerril et al. 2012; Percopo et al 2014; Potvin et al. 2012; Salas et al. 2011) indicate a global distribution of the genus. However, species of *Azadinium* and/or the presence of azaspiracid toxins have not yet been reported for arctic or subarctic areas (Poulin et al. 2011). In the present paper, we present detailed morphological descriptions and sequence data of three new species of *Azadinium* isolated from water samples collected in the North Atlantic between Greenland and Iceland.

Results

1. Species descriptions

Specimens of *Azadinium* were observed in concentrated whole water samples at a number of stations between Greenland and Iceland and around the north-west coast of Iceland (Fig. 1). A total of seven different strains were established. Two strains identified as *Amphidoma languida* (isolated from station 532) and *Azadinium dexteroporum* (isolated from station 526, see Fig. 1) will be presented elsewhere. The other strains were identified to represent three different new species with three strains (4A8, 4B11, A2D11) of *Azadinium trinitatum* sp. nov., and one strain each for *A. cuneatum* sp. nov. (3D6) and *A. concinnum* sp. nov. (1C6) (Tab. 1).

Azadinium trinitatum Tillmann et Nézan, sp. nov. (Figs 2-6)

HOLOTYPE: SEM-stub CEDiT2014H41, prepared from strain A2D11, Figs. 3 B-D, 5C, E, I, 6E; interpretative figure (ICN Art. 44.2.): Fig. 4.

The strain A2D11 of *A. trinitatum* has been deposited at SCCAP, strain K-1883.

ISOTYPE: Formalin fixed sample CEDiT2014I42, prepared from strain A2D11.

TYPE LOCALITY: North Atlantic Ocean, off Iceland, 64° 43.00’ N, 24° 01.50’ W

HABITAT: marine plankton, sub-Arctic

ETYMOLOGY: The epithet is derived from the Latin term “trinitas” = triad, trinity. This was inspired by the fact that the species was available as three different clonal strains, and combine morphological characters of the first three described species of *Azadinium*, *A. spinosum* (the spine, albeit rudimentarily present), *A. obesum* (the shape, shape of the sulcal region), and *A. poporum* (the approximate position of the ventral pore).

The following descriptions and micrographs were compiled from studying all three strains (4A8, 4B11, A2D11), which were indistinguishable with respect to all morphological details identifiable in light and electron microscopy. Cells of *A. trinitatum* were ovoid and dorso-ventrally compressed. Freshly formalin preserved cells of strain A2D11 ranged from 11.3-16.6 µm in length (mean length: 14.1 ± 0.8 µm, n = 120) and 7.1-11.5 µm in width (mean width 9.2 ± 0.8 µm, n = 120), with a mean length/width ratio of 1.5. The episome, which was higher than the hyposome, terminated in a conspicuous apical pore complex (APC) (Fig. 2). The hyposome was rounded, slightly asymmetrical, and having its largest part slightly shifted to the cells' right lateral side. A small antapical spine was visible in LM occasionally (Fig. 2 B-C). The cingulum was descending counter-clockwise, displaced by about the half of its width. It was deeply excavated and wide (1.8-2.4 µm), occupying about one quarter of the cell length.

A presumably single chloroplast was parietally arranged, lobed, and exhibited band-shaped connections extending into the epi- and hyposome (Fig. 2 B-D, H-K). Generally, one large pyrenoid with a starch sheath (visible as a ring-like structure) was located in the episome (Fig. 2 A-C, E). Whereas the pyrenoid was always located in the episome, the shape and number was found to be slightly variable (Fig. 2 F-G). For strain 4A8, a careful examination of 610 cells prepared from a substrain grown at 15°C yielded 582 cells with a single pyrenoid and 28 cells with two pyrenoids. Among 615 cells inspected for strain A2D11, a single pyrenoid was seen in 539 cells, whereas two pyrenoids were detected in 76 cells. In a substrain of 4B11, the amount of cells with two pyrenoids was higher (114 of 600 cells). For all these observations, the presence of two pyrenoids was not related to cells prior to (as potentially indicated by an enlarged cell width) or during cell division. In addition to pyrenoid(s), cells may have a number of large grains both in the epi- and hyposome, which differed from pyrenoids in the absence of a clear starch shield covering them (Fig. 2 E). The large nucleus was spherical, ovoid through distinctly elongated and was located in the hyposome (Fig. 2 H-K).

Thecal plates of *A. trinitatum* were stainable and were identified with calcofluor white (Fig. 2 L). However, the complete plate pattern was more easily determined by SEM (Figs 3, 5-6). The basic thecal plate arrangement was: Po, cp, X, 4´, 3a, 6´´, 6C, 5S, 6´´´, 2´´´´ (Fig. 4). The four apical plates were relatively small. Plate 1´ showed an ortho-pattern and was slender and almost symmetrical with small sutures to plates 2´ and 4´. In its posterior part, 1´ was narrow with sutures running almost parallel to the sulcal area (Figs 3 A-C, 5 A, C). Comparing the small lateral apical plates 2´ and 4´, the right plate 4´ was slightly larger and extending more to the right lateral side (Fig. 5 A-F). Dorsal apical plate 3´ was hexagonal, small, and with slightly variable length of the suture to the intercalary plate 2a (Fig. 5 A, B, D-F). Of the three intercalary plates, the left (1a) and right (3a) plates were relatively large. Due to the small size of the apical plates, they almost reached the pore plate anteriorly. The mid intercalary plate 2a was small and tetragonal. Generally, it was longer than wide, but the shape was variable among cells. The six precingular plates were roughly similar in size, with plate 1´´ as the widest and plates 2´´ and 4´´ as the narrowest. Plate 1´´ was in contact with an intercalary plate (1a) and thus in contact with four epithecal plates, whereas plate 6´´ was separated from plate 3a by the apical plate 4´ (Fig. 5 A-B).

The apical pore was rounded through ellipsoid (mean width: 0.56 ± 0.04 µm, mean length: 0.66 ± 0.06 µm, n = 10, size measurements using SEM images), located in the middle of the pore plate (Po), and covered by a cover pate (cp) (Fig. 5 G-I). A conspicuous rim bordered the dorsal and lateral margins of the pore plate adjacent to apical plates 2´, 3´, and 4´, but was lacking ventrally, where the pore plate abutted the first apical plate and the X-plate. The apical pore was connected through a finger-like protrusion to the small X-plate, which deeply invaded the first apical plate (1') with its posterior part. Shape and anterior borderline of the X-plate could be seen from interior views of the cell (Fig. 5 I). As a conspicuous part of the apical pore complex, a large (mean outer diameter: 0.31 ± 0.03 µm, n = 12) and distinct pore, designated as ventral pore (vp), was located at the left lateral side of the pore plate. This pore

mainly laid within a pocket of the first apical plate and contacted the 2´ plate and the pore plate (Fig. 5 G-H).

The hypotheca consisted of six postcingular and two antapical plates (Fig. 6 A-B). All postcingular plates were tetragonal and similar in shape, but slightly variable in size. Of the two antapical plates, the 2´´´´ plate was distinctly larger with an oblique running suture to plate 1´´´´, which was slightly more anterior in position (Fig. 6 A-B). A short spine could be detected on the second antapical plate (Fig. 6 A-C).

The cingulum was wide, descending, and displaced by about half of its width. Narrow cingular lists were present. The cingulum was composed of six comparably sized plates, except for plate C6 that was more slender than the others (Fig. 6 C-D). Furthermore, this plate was asymmetric in shape, with a conspicuous extension partly covering the sulcal area and thus giving the flagellar pore area a comma-shaped appearance.

The deeply concave sulcus (Fig. 6 C, E) consisted of a large anterior sulcal plate (Sa) that with a broad to slightly pointed anterior side partly invaded the epitheca, and a large posterior sulcal plate (Sp), that extended two-thirds of the line from the cingulum to the antapex. The left sulcal plate (Ss) was broad, located anterior to Sp and abutted plates 1´´´, C1, Sa, Sd, Sm, Sp, and C6. The right sulcal plate (Sd) abutted sulcal plates Ss and Sm, as well as cingular plate C6. The median sulcal plate (Sm) contacted sulcal plates Sa, Ss and Sd (Fig. 6 E-F). These plates had apparently complex three-dimensional morphologies, with large flanges invading into the hypotheca (Fig. 6 F).

The surface of all thecal plates was smooth but irregularly covered by few pores of different size (e.g. arrows in Fig. 5 B). Larger pores ranged in size from 0.11-0.14 µm (mean 0.12 ± 0.01, n = 14), whereas the outer diameter of small pores ranged from 0.07-0.09 µm (mean 0.08 ± 0.01 µm, n = 12). Pores were particularly abundant on the apical plates and most numerous on the large intercalary plates, whereas plate 2a invariably was free of pores (Fig. 5). Both pre- and postcingular plates only had few pores. On postcingular plates these were

mainly located close to the cingulum (Fig. 6 A). Occasionally, small pores were found in small clusters occurring mainly on the cingular plates (Fig. 6 F). There were only few pores on the antapical plates, mainly located around the antapical spine (Fig. 6 A). In sulcal plates, a row of pores was typically present on the left anterior part of Sa (Fig. 6 E-F), although it was often difficult to observe. A small group of pores was located both on lateral sides of Sp and in the middle of Ss, whereas the small sulcal plate Sm and Sd were free of pores.

The characteristic overlapping pattern of thecal plate margins, individually identified for each suture mainly by available interior views of the theca (not shown), is indicated in Figure 4 C-D. In the epitheca, the most ventral plate 1′ was overlapped by all adjacent plates except for the pore plate, whereas the almost mid-dorsal precingular plate 3″ was identified as the "keystone plate" (i.e., a plate overlapping all its neighbours: Fig. 4 C). Within the apical series, the dorsal plate 3′ was overlapped by both adjacent apical plates 2′ and 4′. The small median intercalary plate 2a was overlapped by all adjacent plates. In the cingular and postcingular series, we identified plates C3 and 4‴ as keystone plates, respectively (Fig. 4 D). On the right-ventral side, the last cingular plate C6 was overlapped not only by the C5 plate but also by the anterior sulcal plate (Sa) (Figs 4 C, 6 F).

In our strains, a number of deviations from the typical plate pattern shown in Figure 4 were observed (Figs S1 and S2). Variations in plate pattern primarily consisted of additional sutures between the epithecal plates (Fig. S1 A-I), although variation in number of hypothecal plates were also observed (Fig. S1 J-L). As a rare exception, a penta-configuration of plate 2a was observed (Fig. S2 A). The shape of plate 1´ was variable and was very slender in its proximal part occasionally (Fig. S2 B-C). Although not explicitly quantified, a significant number of specimens had a very short or rudimentary spine, or a spine was completely lacking (Fig. S2 D-I). The position of the ventral pore was consistent but among hundreds of inspected cells, four exception were found nevertheless, in which the pore was displaced posteriorly (Fig. S2 J-M).

Azadinium cuneatum Tillmann et Nézan, sp. nov. (Figs 7-12)

HOLOTYPE: SEM-stub CEDiT2014H43, prepared from strain 3D6; Figs 8 A-D, 10 B-E, 11 D, 12 C-D; interpretative figure (ICN Art. 44.2.): Fig. 9.

The strain 3D6 of *A. cuneatum* has been deposited at SCCAP, strain K-1882.

ISOTYPE: Formalin fixed sample CEDiT2014I44, prepared from strain 3D6.

TYPE LOCALITY: North Atlantic Ocean, off Iceland, 65° 27.00' N, 24° 39.00' W

HABITAT: marine plankton, sub-Arctic

ETYMOLOGY: The epithet is inspired by the distinct shape of the first apical plate, which is wedge-shaped in its distal part (lat.: cuneatus = wedge-shaped).

Cells of *A. cuneatum* were ovoid and slightly dorso-ventrally compressed. Cell size of freshly formalin preserved cells ranged from 11.2-16.9 µm in length (mean 14.2 ± 1.0, n = 188) and from 8.3-12.7 µm in width (mean 10.8 ± 1.0, n = 188), with a mean length/width ration of 1.3. The episome was higher than the hyposome, and it terminated in a conspicuous apical pore complex of a concave shape (Fig. 7). The generally rounded hyposome could be flattened and generally was slightly asymmetric with the longest part displaced to the cells' right lateral side. The subequatorial located cingulum was broad and conspicuous in LM (Fig. 7 B, G, I). A presumably single chloroplast was parietally arranged, lobed, retiform in the episome, and extending into the epi- and hyposome (Fig. 7 D, H, J-K). A large pyrenoid with a starch sheath (visible as a ring-like structure) was predominantly located in the episome (Fig. 7 D, G, I). However, there was some variability for both the number and position of pyrenoid(s) (Fig. 7 E-F). Among 611 cells of a culture grown at 15°C, 573 cells had a single pyrenoid located in the episome, 19 cells had a single pyrenoid located in the hyposome, 6 cells had a

single pyrenoid located in the cingular area, 11 cells had two pyrenoids both located in the episome, and two cells had two pyrenoids, one of which was located in the episome and one in the hyposome. For another strain grown at 10°C, a comparable quantification of 621 cells yielded 577 cells with a single pyrenoid in the episome, 22 cells with a single pyrenoid located in the hyposome, and 22 cells with two pyrenoids, all of them located in the episome. The large nucleus was located in the hyposome/cingular region and typically was spherical through ovoid, but elongated nuclei extending into the episome could also be observed (Fig. 7 H, J).

SEM analysis of *A. cuneatum* (Figs 8-12) revealed the basic thecal plate pattern as Po, cp, X, 4´, 3a, 6´´, 6C, 5S, 6´´´, 2´´´´ (Fig. 9). Among the 4 apical plates, the lateral and dorsal plate 2´, 3´, and 4´ were relatively large and of equal size (Fig. 10 A-B). The lateral apical plates 2´and 4´ largely extended into the ventral area accounting for about half of the epitheca's height (Fig. 10 C-D). The first apical plate was rhomboid and almost symmetric in its posterior part, but was distinctly asymmetric in its anterior part, which was unequally elongated and tapered on its left side reducing the pore plate. Three intercalary plates were symmetrically arranged on the dorsal side (Fig. 10 A, E-F). As the most abundant arrangement, the distinctly smaller central intercalary plate 2a was tetragonal and almost symmetrically located above plate 3´´ (Fig. 10 E), but with a slight displacement to the cells' right lateral side. A penta-configuration (i.e., plate 2a was pentagonal) was abundant, but with plate 2a in contact to 3´´ and 4´´ and with the suture between 3´´ and 4´´ shifted towards the dorsal centre (Fig. 10 F). In cells of a single preservation step, 84 of 123 specimens had a tetragonal 2a, whereas the plate had a penta-configuration in 39 specimens. In cells of another preservation step, plate 2a was tetragonal in 27 and pentagonal in 18 of 45 specimens, respectively. The first and last of the six precingular plates were restricted to the ventral area and distinctly separated from (i.e., not in contact to) the dorsal intercalary plates (Fig. 10 A-

D). Plates 6´´ and 4´´ were the narrowest precingular plates, while plate 2´´ was the widest (Fig. 10 A).

The distinct apical pore was circular, tear-drop shaped, or slightly ellipsoid with a mean width of 0.69 ± 0.04 µm (n = 12) and a mean length of 0.85 ± 0.04 µm (n = 10). It was located in the dorsal part of a slightly elongated pore plate and covered by a cover plate (Figs 10 A-B, 11 A-F). Because of the invading tip of plate 1´, the pore plate was distinctly asymmetric. It was bordered by a rim formed by the apical plates along the sutures of 2´-4´ and the pore plate. Rarely, the rim extended along the left lateral side between the suture of plate 1´ and 2´ (Fig. 11 E). An X plate was located between the first apical and the pore plate, which was clearly visible from interior views as a small and slightly elongated plate. It invaded both the pore plate and the 1´ plate, but without reaching the apical pore (Fig. 11 F), as it might be the impression from exterior view. Cover plate and X-plate were connected by a characteristic finger-like protrusion (Fig. 11 A-E). A distinct pore with a mean outer diameter of 0.33 ± 0.02 µm (n = 12) was located on the left lateral side of the pore plate and at the tip of the elongated left anterior part of the first apical plate on the suture between the pore plate and the apical plate 2´ (Fig. 11 A-E). Despite its almost apical position, we denominate this pore as the "ventral pore" (vp).

Six postcingular and two antapical plates formed the hypotheca (Fig. 12 A, B). Among the six postcingular plates, plate 5´´´ was the widest. Plates 1´´´ and 6´´´ were in ventral position and of the same small size as the most dorsal plate 4´´´. Plate 3´´´ was the plate of the postcingular series in contact to both antapical plates. Of the two antapical plate, plate 2´´´´ was about double the size of the 1´´´´ plate (Fig. 12 A-B).

The subequatorial cingulum was wide, descending, displaced by about half of its width, and was composed of six plates (Fig. 12 C). It exhibited narrow cingular lists formed by the posterior margins of the precingular plates and anterior margins of the postcingular plates (Fig. 8 A-D). The most dorsally located C3 and the lateral cingular plates C2 and C4 were

wide and the ventrally located last cingular plate C6 forming the right ending of the sulcal area was the narrowest cingular plate (Fig. 12 C).

The excavated sulcal area was formed by five plates (Fig. 12 D-E). The large anterior sulcal plate (Sa) partly invaded the epitheca, and the large posteriour sulcal plate (Sp) extended about half the line from the central sulcus to the antapex (Fig. 8 A-B). The left sulcal plate (Ss) was very broad and ran along the line from plate C1 to C6. Two smaller and centrally located sulcal plates (Sm and Sd) formed a concave central pocket (Fig. 12 D-E).

The plates of *A. cuneatum* were smooth with irregularly distributed small pores (Fig. 8) of slightly varying size (range: 0.08-0.14 µm; mean: 0.11 ± 0.02 µm, n = 23). On the epitheca, pores were concentrated on the anterior area of the apical plates (Fig. 10). The median intercalary plate 2a was consistently free of pores. Generally, pores were individual or arranged in small groups of up to eight. On both post- and precingular plates, pores were arranged along the boundary to the cingulum (Fig. 12 A, 10 E). Small groups of pores were present on sulcal plates Sa, on both lateral sides of Sp, and as a distinct group of pores located in the middle of the broad Ss plate (Fig. 8 A-B).

The pattern of plate overlap was identified individually for each suture mainly by interior view (not shown) and is depicted in Figure 9 C-D. As most characteristic features, plate 3´ was overlapped by its neighbouring apical plates 2´ and 4´, plate 2a was overlapped by all adjacent plates, and plate C6 was overlapped by the central sulcal plate Sa. As keystone plates of *A. cuneatum*, we identified 3´´, C3 and 4´´´ for the precingular, the cingular, and the postcingular series, respectively.

Plate variability observed in the culture of *A. cuneatum* mainly occurred in the epitheca. The presence of both quadra- and penta-configuration of plate 2a (Fig. S3 A-C) was already described before. In addition, only two intercalary plates may rarely be present (8 out of 131 cells) (Fig. S3 D-I). Other epithecal variants and a hypothecal reduction of postgingular plates are illustrated in Figure S4 A-E. The position of the ventral pore for *A. cuneatum* was

consistent but among hundreds of investigated cells, four exceptions were found nevertheless, where the pore – together with varying degrees of a reduction of the anterior elongation of plate 1´ – was displaced posteriorly (Fig. S4 F-I).

Azadinium concinnum Tillmann et Nézan sp. nov. (Figs. 13-17)

HOLOTYPE: SEM-stub CEDiT2014H45, prepared from strain 1C6; Fig. 14 A-B; interpretative figure (ICN Art. 442.): Fig. 15.

The strain 1C6 of *A. concinnum* has been deposited at SCCAP, strain K-1881.

ISOTYPE: Formalin fixed sample CEDiT2014I46, prepared from strain 1C6.

TYPE LOCALITY: North Atlantic Ocean, Irminger Sea, off Greenland, 62° 13.95' N, 37° 27.31' W

HABITAT: marine plankton, sub-Arctic

ETYMOLOGY: The Latin adjective "concinnus" (= beautiful, elegant, harmonious, "skilfully put together") reflects the concinnity of this delicate and petite species.

Cells of *A. concinnum* were very small, slender and only slightly dorso-ventrally compressed. The episome was distinctly longer than the hyposome, slightly concave to almost linear in outline, and terminated in a prominent apex (Fig. 13 B). The rounded hyposome terminated in a conspicuous antapical spine in median or laterally displaced position (Fig. 13 B-E). The cingulum was very broad and deeply excavated. Cell size was 8.0-11.5 µm in length (mean = 9.5 ± 0.7, n = 175) and 5.6-8.3 µm in width (mean = 6.6 ± 0.5, n = 175), resulting in a mean length/width ration of 1.4. A presumably single chloroplast was present, which was lobed and extending from the episome into the hyposome (Fig. 13 F-I). In LM, there was no indication for the presence of a pyrenoid surrounded by a starch shield. Occasionally, a number of

spherical bodies of varying size was seen in both the epi- and hyposome (Fig. 13 D-F). A large and almost spherical nucleus was located in the subequatorial cingular region (Fig. 13 G, I).

Thecal plates of *A. concinnum* probably were weakly developed and delicate, which made it almost impossible to obtain complete cell views of trim specimens. The basic plate pattern of *A. concinnum* as inferred from SEM images (Figs 14-17) was Po, cp, X, 4´, 3a, 6´´, 6C, 5S, 6´´´, 2´´´´ (Fig. 15). Four small apical plates surrounded the apical pore (Fig. 16). The first apical plate, which was extending half the line from the apex to the cingulum (Fig. 14 A), was narrow, showed sutures to the apical plates 2´ (shorter) and 4´ (longer) of slightly unequal length (Fig. 16 B), and was rectangular in its posterior part (Fig. 16 A). The sutures of plate 3´ to its neighboring apical plates were very short so that the epithecal intercalary plates almost approached the pore plate (Fig. 16 A, D). The series of three small intercalary plates were located dorsally and together formed an almost circular area with the apical plates around the apical pore. Plate 2a was distinctly smaller than the other intercalary plates and was of pentagonal shape and symmetrically in contact to two precingular plates. All six precingular plates were of equal size and were arranged symmetrically with the suture between plate 3´´ and 4´´ in mid-dorsal position.

An upward arched arrangement of the apical plates gave rise to the distinct and stepped appearance of the apex (Figs 14 A-B, 16 F). The apical pore was spherical through slightly elongated (mean width: 0.47 ± 0.02 µm, mean length: 0.56 ± 0.02 µm, n = 15), covered by a cover plate, and centrally located in a horseshoe shaped pore plate (Fig. 16 A, H-I). At its lateral and dorsal parts, a thick rim bordering the pore plate extended ventrally along the sutures of plate 1´ with its adjacent apical plate 2´ and 4´ (Fig. 16). A small and circular X-plate was visible from interior views (Fig. 16 I), which did not invade the first apical plate and which was shifted to the cells' right lateral side adjacent to the ventral pore (see below). A finger-like protrusion connecting the X-plate and the cover plate was characteristically bended

to the cells' right lateral side inserting at the cover plate in a subequatorial position (Fig. 16 G- H). A distinct "ventral pore" was located on the right ventral side of the pore plate with a distortion of the suture Po/4´, the latter one characteristically accentuated by the recessed run of the rim (Fig. 16 G-H).

The hypotheca was composed of six postcingular and two antapical plates (Fig. 17 A). The first and the last postcingular plates were of similar size, ventrally located, and of distinctly lower height compared to the other postcingular plates. Plate 3´´´ was in contact to both antapical plates. Because of the low height of the ventral postcingular plates, both antapical plates largely extended into the ventral area to almost the same level. Plate 2´´´´ was large and separated by a slightly oblique suture from the smaller first antapical plate. A distinct and approx. 0.95 µm long antapical spine was located on the dorsal part of plate 2´´´´ in the cells median axis or slightly displaced to the cells left lateral side (Fig. 14).

With a width of about 2-2.5 µm, the cingulum of *A. concinnum* was remarkably wide accounting for about a quarter of total cell length. Furthermore, the cingulum was deeply excavated, slightly descending, and composed of six plates (Fig. 17). Of the five sulcal plates, the anterior sulcal plate Sa deeply invaded the epitheca with an elongated and tapered end reaching about half the line to the apex (Figs. 14 A, 17 B, C). The plate Ss running from plate C1 across to plate C6 was broad on its left side but distinctly slender in its right part, which – together with the small central sulcal plates Sd and Sm – formed a deeply concave and egg-shaped central pocket (Fig. 17 B-D).

The surface of thecal plates was smooth with just a very few though conspicuous pores present (Fig. 14). Invariably, the postcingular plates had a single pore located at underlapping margins (see below) of the suture to the neighboring postcingular plates (Fig. 17 A). Consequently, the keystone plate plate 4´´´ (see below) was free of pores. Furthermore, pores were present on both epithecal and hypothecal margins of cingular plates (Fig. 14). Lateral and dorsal apical plates 2´- 4´ were free of pores, as were all precingular plates and the central

intercalary plate 2a (Fig. 16). A single or rarely two or three pores were located on the outer intercalary plates (Fig. 16 D). A characteristic vertical row of 3-5 pores was always present on the first apical plate (Figs 16 A, F-H).

The pattern of plate overlap of *A. concinnum* as inferred mainly from available interior views (not shown) is schematized in Figure 15 C-D. The overlap pattern was identical to the patterns described for *A. trinitatum* and *A. cuneatum*, with plates 3´´, C3, and 4´´´ identified as keystone plates of the precingular, cingular, and postcingular series, respectively.

Variation of plate pattern observed in the culture of *A. concinnum* are summarised in Figures S5 and S6. Plate pattern variability was mainly observed for epithecal plates. The most frequently encountered deviations were a loss of one intercalary plate and/or displacement of intercalary plates providing contact to the pore plate. For *A. concinnum*, no variability in ventral pore position was observed among hundreds of cells investigated.

2. Molecular Results

The SSU+ITS+LSU alignment was 4609 bp long and comprised 1813 parsimony informative sites (39%, mean of 11.62 per OTU). Tree topologies were largely congruent, irrespectively whether the Bayesian or the ML algorithm was applied. Many nodes showed high if not maximal support values. Figure 18 shows the best-scoring ML tree, in which the Amphidomataceae were monophyletic (99LBS, 1.00BPP) with respect to the outgroup. The internal topology of the Amphidomataceae was not fully resolved, but showed a sister group relationship between *Amphidoma languida* and *Azadinium* (55LBS). As inferred from very short branches in the molecular tree, the different accessions of the three new species did not show notable variation of rRNA copies.

The new species had different phylogenetic positions in the molecular tree: *Azadinium concinnum* (100LBS, 1.00BPP) constituted the sister species of the remainders of *Azadinium* (100LBS, 1.00BPP). Within *Azadinium*, a sister group relationship consisted between *A.*

cuneatum (100LBS, 1.00BPP) and a clade comprising the species *A. dalianense*, *A. obesum*, *A. poporum*, *A. spinosum*, and *A. trinitatum* (1.00BPP). *Azadinium trinitatum* had its closest relative in a yet undescribed symbiotic partner of the radiolarian *Acanthochiasma* Krohn, 1861 (94LBS, 1.00BPP) and together, they were closely related to a clade comprising *A. dalianense*, *A. obesum*, *A. poporum*, and *A. spinosum*.

3. AZA analysis

Using SRM, none of previously described AZAs (AZA-1 to -12 and AZA-33 to -41) were found in *A. concinnum* (1C6), *A. cuneatum* (3D6), and *A. trinitatum* (4A8, 4B11, A2D11) at a detection limit of 1.1 pg on column, which corresponds to a limit of detection at cellular level of 0.020-0.026 fg cell^{-1} for *A. trinitatum* (slightly different for the different strains due to different biomass of the samples), 0.015 fg cell^{-1} for *A. cuneatum*, and 0.012 fg cell^{-1} for *A. concinnum*.

For detecting putative precursor masses of the characteristic CID-fragments *m/z* 348 and *m/z* 362 of AZAs, precursor ion experiments were also negative for all three species. However, the precursor on mode is approximately a hundred times less sensitive than the SRM mode and strictly speaking, it did not allow for exact quantitative measurement. Considering a conservatively determined “detection limit” of 0.2 ng on column, this represented a cellular detection limit of unknown AZA variants of 2.5 to 5 fg.

Discussion

Plate pattern analysis clearly shows that all strains reported here belong to the Amphidomataceae in general and to *Azadinium* in particular. Moreover, our analysis reveals unique morphological features justifying the description of three new species, and this has been confirmed by the phylogenetic analysis based on concatenated sequence data of the SSU, ITS, and LSU rRNA. Already with the description of the first *Azadinium* species, the presence of an antapical spine and the position of a ventral pore have been highlighted as important morphological features characterizing different species (Tillmann et al. 2009, 2010, 2011). With the present work and now distinguishing 10 species of *Azadinium*, this notion is reinforced with the position of the ventral pore identified as one of the most distinctive characters (Tab. 3). Generally, the position of the ventral pore seems to be a distinct and species-specific character for species of *Azadinium*, although a deviating position of the ventral pore can be found very rarely (Potvin et al. 2012; this study: Figs. S2, S4 supplementary material). In particular, the three new species described here can be distinguished from other species of *Azadinium* by a number of features as follows:

A. trinitatum

The main characteristic and distinctive features of *A. trinitatum* are the unique combination of the location of the ventral pore (located at the left distal end of the pore plate), the presence of three epithecal intercalary plates, and the presence of an antapical spine. As it is reflected in its name, *A. trinitatum* combines morphological characters of the first three described species of *Azadinium*. While sharing the presence of an antapical spine with *A. spinosum*, the slightly more obese cell shape, the distinctly slender posterior part of plate 1´, and the outline of the sulcal region more closely resembles *A. obesum*. With the third species, *A. poporum*, and also with *A. dalianense* (although it has 3 apical and 2 intercalary plates), *A. trinitatum* shares the

position of the ventral pore on the left side of the pore plate (Tab. 3). However, a detailed comparison of the pore plate and vp arrangement (Fig. 19) indicates that the ventral pore is located more in a cavity of the pore plate in *A. poporum*. For *A. dalianense*, the ventral pore is located at the junction of the pore plate and the first two apical plates in a cavity mainly formed by the second apical plate and the pore plate. The suture between Po and 1´ is almost symmetric in *A. dalianense*. For *A. poporum*, the pore plate is slightly asymmetric: The left side of the suture Po/1´ with the vp is located closer to the apical pore than the right side. In contrast, the ventral pore is located more in a cavity of the 1´ plate at the tip of an elongated side of the pore plate in *A. trinitatum*. The pore plate is asymmetric but here, the left side of the suture Po/1´ with the vp is more distant from the apical pore than the right side (Fig. 19). The elongated left side of the Po plate resembles the asymmetric and elongated shape of the Po of *A. dexteroporum* (Percopo et al. 2013) but here, the elongated side of Po is at right.

The presence/absence and development (in case of *A. caudatum* var. *margalefii* or *caudatum*, respectively) of an antapical spine has also been emphasized in distinguishing species of *Azadinium* (Tab. 3). For all three strains of *A. trinitatum*, we identify a short antapical spine, but we find this trait to be variable. Indeed, the presence of a spine in our cultures is predominant, but such structure is rudimentarily present or definitely missing in many cells (see Fig. S2 D-I). More prominent spines are described for *A. spinosum*, *A. caudatum*, *A. polongum*, *A. dexteroporum*, and described here for *A. concinnum*. A sporadic but significant presence of a more rudimentary spine is also described for *A. dalianense* (Luo et al. 2013). In any case, more targeted studies of cultivated material are needed to evaluate potential effects of culture conditions in *Azadinium* (not restricted to spine formation but also including clonal plate pattern variability).

Both morphological and molecular data do not allow doubts upon *A. trinitatum* representing a novel species, but the taxon might have been illustrated before as "*Gonyaulax gracilis*" (Schiller 1935) (not validly published: ICN Art. 38.1., no description or diagnosis). Later,

Holmes (1956) reported from a “small *Goniaulax* probably identical with *G. gracilis* Schiller” in the southern central Labrador Sea. We cannot exclude that his figure 28 (p. 61) is a species of *Azadinium* and particularly *A. trinitatum*. However, the small spine at the antapex is lacking in his illustration, while it is visible even using LM in *A. trinitatum*. Later, Bérard-Therriault et al. (1999) provided additional figures of this species (pl. 90) showing dinophytes with a great similarity to *Azadinium* in terms of size, shape, and outline of the sulcal area. One of the specimens depicted therein has an antapical spine and another cell obviously has no spine. Other details are not provided, so it even remains uncertain whether the dinophytes they reported from eastern Canada in fact represent species of *Azadinium*. Nevertheless, it is possible that they represent *A. trinitatum* based on the general appearance of these cells. The similarity of the locality of the specimen depicted by Bérard-Therriault et al. (1999), the Canadian Arctic and our record of *A. trinitatum* from Iceland, generally would support this view.

A. cuneatum

A. cuneatum differs from all other species of *Azadinium* by a very particular first apical plate, which is asymmetrically elongated and tapered on its left lateral side reducing the pore plate. Differently from all other species of *Azadinium*, the ventral pore is located in the middle of the pore plate at the tip of the elongated 1´ plate and invading both Po and the second apical plate 2´. In addition, *A. cuneatum* is characterized by the exceptional large size of the apical plates (Tab. 3). Furthermore, the first precinguar plate is not in contact with the first intercalary plate, a feature that *A. cuneatum* is sharing with *A. obesum* and *A. concinnum* only (Tab. 3).

A tetra-configuration of the intercalary plate 2a (i.e., plate 2a is tetragonal and in contact with the 3´´ plate) is the most abundant configuration for *A. cuneatum*. However, a penta-configuration (i.e., plate 2a in contact to five other plates, including both 3´´ and 4´´) is

present in many cells as well. In most cases, contact of 2a to 3´´ and 4´´ is asymmetric (a wider suture of 2a and 3´´: Fig. 10 F), but an almost symmetric arrangement is also observed, albeit rarely (Fig. S3 C). A symmetric arrangement of precingular plates and a penta-configuration of plate 2a have been described here for the new and first branching species *A. concinnum*. The presence of both tetra- and penta-configuration of plate 2a within a single species has also been described for field populations of *Peridiniella danica* (Paulsen) Okolodkov et J.D.Dodge (Okolodkov and Dodge 1995) although here, conspecificity of the different types is not confirmed.

For many cells (in one preparation quantified as 6%), the presence of only two intercalary plates is noted in *A. cuneatum* (Fig. S3 D-I). If the absence of pores is indicative for the "true" 2a plate, then it is indicated that both possibilities, loss of the first and loss of the last intercalary plate are likewise plausible. An consistent presence of only two intercalary plates has been described as the main character of *A. dalianense*, and here in connection with a concurrent reduction of the apical series to three apical plates (Luo et al. 2013).

A. concinnum

Azadinium concinnum is unique among species of *Azadinium* by an elongated anterior sulcal plate ranging far into the epicone, by large and symmetric precingular plates, by very small apical and epithecal intercalary plates, and by having a penta-configuration of plate 2a as the most common configuration. Although size ranges of most species of *Azadinium* do overlap, *A. concinnum* is of particularly small size, almost identical in size with the small species *A. dexteroporum* (Tab. 3). *A. concinnum* and *A. dexteroporum* also share the position of the ventral pore on the right side of the pore plate (Tab. 3). However, the pore is located in a pit of the otherwise symmetric pore plate in *A. concinnum*, whereas it is located at the posterior part of an elongated extension of the right side of the pore plate in *A. dexteroporum* (Percopo et al. 2013). A position of the ventral pore on the cells' right lateral side is a feature shared by

A. concinnum with *A. caudatum*, *A. dexteroporum*, and *Amphidoma languida*. In terms of the elongated Sa plate, the large and symmetric precingular plates and the small epithecal intercalary plate with 2a in a penta configuration, there is another species having exactly such features. A small dinophyte species has been described in 1959 as *Gonyaulax parva* Ramsfjell from Atlantic Ocean samples of the central Norwegian Sea and from waters towards Iceland (Ramsfjell 1959). The plate pattern of this species is, anyhow, different from *Gonyaulax* and in fact corresponds to the plate tabulation of *Azadinium*. Subsequently, the species should be transferred to *Azadinium* (Tillmann et al. 2009), but this will be performed in a further taxonomic study. In any case, *A. concinnum* differs from *G. parva* by the presence of the antapical spine, by the smaller size, and by a more slender cell shape. Based both on the very similar features of the precingular plates (symmetrical arrangement and size), and on the small size of all apical and intercalary plates, we expect a very close relationship between *A. concinnum* and *G. parva*. Presence and/or position of the ventral pore have not been reported, because LM observations of *G. parva* only are available at this moment in time.

The presence of six large and symmetrical precingular plates, and a small size of the remaining epithecal plates of *A. concinnum*, are features also typical for *Amphidoma* (Dodge and Saunders 1985; Tillmann et al. 2012a). Moreover, conspicuous pores are consistently located at the sutures of the postcingular plates of *A. concinnum* and *A. languida* as well. At a first glance, there is a large difference in epithecal plate arrangement, with *Amphidoma* exhibiting six apical plates and no apical intercalary plate, while all species of *Azadinium* have only 3-4 apical plates but 2-3 apical intercalary plates. However, this difference vanishes when the total number of epithecal plates is considered: It is plausible to assume that the intercalary plates of *Azadinium* are homologous to at least some of the apical plates present in *Amphidoma*. Minor displacements of particular epithecal plates have been discussed controversially in the past also for other dinophyte species such as *Protoceratium reticulatum* (Claparéde et Lachmann) Buetschli [= *Gonyaulax grindleyi* P.Reinecke, Gonyaulacales;

Dodge (1989); Hansen et al. (1996/97)]. The taxon has been described with both 4´, 0a (Wołoszyńska 1928) and 3´, 1a (Reinecke 1967), respectively. Hansen et al. (1996/97) likewise circumscribed the epithecal plate pattern of the species as 3´, 1a, 6´´, but emphasized as well that nearly 50% of cells of a field sample show contact between 1a and the pore plate (i.e., 4´, 0a, 6´´ in a strict Kofoidean formula).

Plate overlap

All three new species share the same imbricate plate overlap pattern. Generally, plate overlap patterns may reflect functional aspects of ecdysis and/or archeopyle types of coccoid cells, and help to determine plate homologies. A number of uncommon imbrications have been identified for the genus *Azadinium*, i.e. the most dorsal apical plate 3´ is overlapped by the adjacent apicals 2´ and 4´, the median intercalary plate 2a is overlapped by all adjacent plates, and the large anterior sulcal plate overlaps the last cingular plate C6 (Luo et al. 2013; Nézan et al. 2012; Tillmann and Elbrächter 2010; Tillmann et al. 2012a, 2012b), and all of these pattern have been confirmed here for the three new species.

Pyrenoids

For a number of species, stalked pyrenoid(s) are visible in LM because of a distinct starch cup. The presence/absence, position, number, and ultrastructure of pyrenoids have been regarded as useful characters to delimitate taxa (Schnepf and Elbrächter 1999; Tillmann et al. 2011) and has in particular been discussed as a powerful feature visible to differentiate species of *Azadinium* in LM (Tillmann et al. 2011). *A. concinnum* consistently lacks pyrenoid(s) identifable by a distinct starch cup, but pyrenoid(s) are variable in *A. trinitatum* (both number and position) and *A. cuneatum* (number). Variability in pyrenoid number and position has also been reported for *A. dalianense*, indicating that these traits are of limited

value for species delimitation. In any case, more detailed information (including ultrastructure) related to the pyrenoids of *Azadinium* is needed.

Evolution

The Amphidomtaceae are always retrieved monophyletic in molecular phylogenetic analyses (Gu et al. 2013a; Tillmann et al. 2012a, 2012b), although the sister group has not be determined reliably at this moment in time. This challenges the interpretation of character evolution within the group. Therefore, it remains unresolved whether the epithecal plate pattern is derived either in *Amphidoma* (six apical plates, no intercalary plates) or in *Azadinium* (four apical plates, three intercalary plates), because outgroup comparison is not possible. *Azadinium concinnum* is the first branching species of *Azadinium* and shows some plate pattern variability, at least in our strain. A number of these variants can be interpreted either as loss of a single intercalary plate and/or as a displacement of a single intercalary plate getting in contact with the pore plate (Figs S5 and S6; see above). This may support a scenario, under which epitheca formation is ancestral in *Azadinium* and derived in *Amphidoma* (Fig. 20). However, monophyly of the former including *A. concinnum* should be treated with caution the molecular trees given.

The position of the ventral pore either on the left or on the right lateral side of the dinophyte cell appears not only as a diagnostic, but also phylogenetically informative trait. With the exception of *A. polongum*, the species with a ventral pore on the left lateral side constitute a monophyletic group, while the members with a ventral pore on the right lateral side are paraphyletic. This makes an evolutionary displacement of the ventral pore from the right to the left lateral side plausible as inferred from the molecular phylogenetic trees. However, the ventral pore located on the left lateral side in *A. polongum* must then be interpreted as result of an independent development. The distribution of an antapical spine does likewise not match entirely with the molecular phylogenetic trees. The first four branching lineages

consistently include species with such a structure, providing evidence that a spine belongs to the bauplan of the Amphidomataceae. However, the members lacking a spine do again not constitute a monophyletic group, and its loss must be considered as result of independent evolutionary events. Presence / absence of a spine may vary even within species (i.e., *A. dalianense*), indicating the evolutionary plasticity of this trait.

Distribution and Toxins

Azadinium has been described from the North Sea, although knowledge on the biogeography currently is rather limited and patchy. However, there is growing evidence that *Azadinium* probably has a world-wide distribution: It has been recorded from the warm Pacific Ocean off Mexico (Hernández-Becerril et al. 2012), to form blooms along the Argentinean South Atlantic shelf (Akselman and Negri 2012), to occur along the Asian Pacific coast (Gu et al. 2013b; Potvin et al. 2012), is now known from the Mediterranean (Percopo et al. 2013), has been included in the check list of Black Sea phytoplankton (http://phyto.bss.ibss.org.ua/wiki/Azadinium_spinosum), and is verified in SEM plankton samples from the open Indian Ocean (pers. com., Consuelo Carbonell-Moore, Oregon State Univ., USA). Here, we now report on a range extension of *Azadinium* to a sub-polar area (Irminger Sea, northern Atlantic Ocean off Iceland). This comes not too much as a surprise given the recent record of *A. spinosum* and *A. polongum* from the Shetland Islands (Tillmann et al. 2012b), which are located in the northernmost part of the North Sea and are largely influenced by the North Atlantic Ocean. In addition, *G. parva* (which almost certainly is a species of *Azadinium*, see above) has been recorded from the central Norwegian Sea towards Iceland (Ramsfjell 1959), while "*G. gracilis*" which probably also refers to a species of *Azadinium*, originates from the Canadian Arctic (Bérard-Therriault et al. 1999; Holmes 1956). We do not yet have quantitative data of *Azadinium* species from the Irminger Sea and Iceland, but onboard LM of concentrated bottle samples indicate a generally low abundance of

Azadinium-like cells. More detailed studies on the seasonal variation, also using molecular probes (Toebe et al., 2013), are needed to provide data on the quantitative importance of these species in cold water ecosystems. With now three new species and the additional record of *A. languida* and *A. dexteroporum* (which will be presented elsewhere), the diversity of the Amphidomataceae in that region seems to be high, especially since our presented findings are based on a single cruise and a limited number of stations.

We failed to detect known azaspiracids and other compounds producing AZA-characteristic MS fragments in all available strains of the three new species. What we know from work with *A. spinosum* is that AZA production in a given strain is constitutive, that toxins are found in significant amounts in the cells at all stages of growth and at all environmental conditions tested so far (Jauffrais et al. 2013). However, we must be aware that toxin production can be variable among strains of a single species. *Azadinium poporum* was reported to be a non-toxigenic species at first (Tillmann et al. 2011) but later, it was proved to produce several different novel AZAs, although with a high strain variability (Gu et al. 2013b; Krock et al. 2012). Moreover, some new Asian strains produce the previously known toxic AZA-2, and – among a total of 22 strains of *A. poporum* analysed so far – four strains without any detectable AZAs are found (Gu et al. 2013b; Krock et al. 2014). Only a single strain of *A. cuneatum* and *A. concinnum* and three strains of *A. trinitatum* are available and have been examined so far, and clearly more strains are needed to evaluate if absence of AZAs is a consistent and species-specific trait of these new *Azadinium* species.

Material & Methods

Isolation and culture

A number of strains of *Azadinium* (i.e., strains A2D11, 4A8, 4B11, 3D6, 1C6) were established from water samples collected at two stations between Greenland and Iceland (station 525: 62° 13.95´ N, 37° 27.31´W; station 526: 64°45.71´N, 29°56.74´W) and three stations off the north-western coast of Iceland (station 532: 65°27.00´N, 24°39.00'W; station 537: 65°10.00'N, 23°26.97'W; station 540: 64°43.00'N, 24°01.50'W) during a cruise aboard the research vessel "Maria S. Merian" in August 2012 (Fig. 1, Tab. 1). One-Liter Niskin bottle samples (10 m depth) from each station was pre-screened (20 µm Nitex gauze), gently concentrated by gravity filtration using a 3-µm polycarbonate filter, and examined using an inverted microscope (Axiovert 200M, Zeiss, Germany). Cells of *Azadinium* (generally rare in the samples) were visually pre-identified at high magnification (640X) based on general cell size and shape, on the presence of a theca and presence of a distinct and pointed apex.

Pre-identified cells were isolated by micro-capillary into wells of 96-well plates filled with 0.2 mL filtered seawater. By this transfer technique, the inclusion of non-target cells is unavoidable. Therefore, each primary well of isolation was partitioned as 10 µL quantities distributed into 20 new wells pre-filled with 0.2 mL filtered seawater. Plates were incubated at 10°C under a photon flux density of appr. 50 µmol m^{-2} s^{-1} on a 16:8 h light:dark photocycle in a controlled environment growth chamber (Model MIR 252, Sanyo Biomedical, Wood Dale, USA). After 4 weeks of growth, plates were inspected for the presence of *Azadinium*-like cells as inferred from the typical size, shape, and swimming behavior of other known *Azadinium* species. From each positively identified well, a clonal strain was established by isolation of single cells by micro-capillary. Established cultures were routinely held at both 10°C and 15°C in an natural seawater medium prepared with sterile-filtered (0.2 µm VacuCap filters, Pall Life Sciences, Dreieich, Germany) Antarctic seawater (salinity: 34 psu, pH

adjusted to 8.0) and enriched with 1/10 strength K-medium (Keller et al. 1987; slightly modified by omitting addition of ammonium ions). All strains are available on request. For toxin analysis, strains were grown in 250 ml plastic culture flasks at 15°C under a photon flux density of 50 µmol m^{-2} s^{-1} on a 16:8 h light:dark photocycle. For each harvest, cell density was determined by settling lugol fixed samples and counting >800 cells under an inverted microscope. Densely grown strains (ranging from 3-11 x 10^4 cells mL^{-1}) were harvested in 4 x 50 mL centrifugation tubes by centrifugation (Eppendorf 5810R, Hamburg, Germany) at 3220 g for 10 min. Each four pellets from a single strain were combined in an microtube, again centrifuged (Eppendorf 5415, 16,000 g, 5 min), and stored frozen (–20°C) until use. Growth and harvest procedures were repeated several times to yield a total number of at least 2 x10^8 cells. Total volume and number of cells harvested for the different strains was: 4A8: 3.3 L, 2.1 x 10^8 cells; 4B11: 4.1 L, 2.6 x 10^8 cells; A2D11: 2.5 L, 2.0 x 10^8 cells; 3D6: 4.7 L, 3.6 x 10^8 cells; 1C6: 8.6 L, 4.6 x 10^8 cells.

All harvests of the different strains were combined in 2 mL methanol and homogenized with a sonotrode (Sonoplus HD 2070, Bandelin, Berlin, Germany) in 70 cycles at 100% power for 70 s. Homogenates were centrifuged (Eppendorf 5810 R, Hamburg, Germany) at 15°C and 3220 x g for 15 min. Supernatants were collected, and pellets twice re-extracted with 1 mL methanol each. Combined extracted were reduced in a rotary evaporator (Büchi, Konstanz, Germany) at reduced pressure and 40°C water bath temperature to a volume < 0.5 mL and were then taken up in acetone to a final volume of 1 mL. The extracts were transferred to a 0.45 µm pore-size spin-filter (Millipore Ultrafree, Eschborn, Germany) and centrifuged (Eppendorf 5415 R, Hamburg, Germany) at 800 x g for 30 s, with the resulting filtrate transferred into a liquid chromatography (LC) autosampler vial for LC-MS/MS analysis.

Light microscopy (LM)

Observation of live or fixed cells was carried out with a stereomicroscope (Olympus SZH-ILLD) and an inverted microscope (Axiovert 200 M, Zeiss, Germany) as well, equipped with epifluorescence and differential interference contrast optics. Light microscopic examination of the thecal plate tabulation was performed on formalin fixed cells (1% final concentration) stained with calcofluor white (Fritz and Triemer 1985). Shape and position of the nucleus was determined after staining of formalin fixed cells with 4'-6-diamidino-2-phenylindole (DAPI, 0.1 µg mL^{-1} final concentration) for 10 min. Photographs were taken with a digital camera (Axiocam MRc5, Zeiss, Germany).

Cell length and width were measured at 1000 x microscopic magnification using Zeiss Axiovision software (Zeiss, Germany) and freshly fixed cells (formalin, final concentration 1%) of strains growing at 15°C.

Scanning electron microscopy (SEM)

For SEM examination of thecal plates, cells from growing strains held at 15°C were fixed, prepared, and collected on 3-µm polycarbonate filters (Millipore) as described by Tillmann *et al.* (2011). Filters were mounted on stubs, sputter-coated (Emscope SC500, Ashford, UK) with gold-palladium, and viewed under a scanning electron microscope (FEI Quanta FEG 200, Eindhoven, Netherlands). Some SEM micrographs were presented on a black background using Adobe Photoshop 6.0 (Adobe Systems, San Jose, CA, USA). SEM micrographs were used for size measurements of various pores.

All material with taxonomic importance (such as type material) was permanently preserved at the same point in time and was deposited at the Senckenberg Research Institute and Natural History Museum, Centre of Excellence for Dinophyte Taxonomy (CEDiT), Germany.

Chemical analysis for azaspiracids and precursor ion experiments

For all strains, a deep analysis for the presence of AZAs was conducted. Samples were analyzed by LC coupled to tandem mass spectrometry (LC-MS/MS) according to the methods described in detail by Tillmann et al. (2009). Selected reaction monitoring (SRM) experiments were carried out in positive ion mode by selecting the following transitions given in Table 2.

Precursors of the fragments *m/z* 348 and *m/z* 362 were scanned in the positive ion mode from *m/z* 400 to 950 under the following conditions: curtain gas: 10 psi, CAD: medium, ion spray voltage: 5500 V, temperature: ambient, nebulizer gas: 10 psi, auxiliary gas: off, interface heater: on, declustering potential: 100 V, entrance potential: 10 V, collision energy: 70 V, exit potential: 12 V.

Molecular phylogenetic analysis

Two optional methods were used to obtain genomic DNA: 1) DNA extraction from an exponentially growing strain of *Azadinium* prior to DNA amplification or 2) direct PCR amplification from a single cell isolated from particular strains. For the first approach, cells from approximately 20 mL of each strain were harvested by centrifugation (4000 rpm, 20 min). The genomic DNA was extracted using the CTAB (*N*-cetyl-*N*,*N*,*N*-trimethylammoniumbromide) method (Doyle and Doyle 1987). For the second approach, each cell was deposited on a glass slide, using a micropipette under the Olympus IMT2 inverted light microscope. Subsequently, each cell was placed in a drop of a sodium thiosulfate solution to decrease the inhibiting effect of the fixative on the PCR (Auinger et al. 2008), rinsed twice in double distilled water (ddH_2O) before transfer to a 0.2-mL PCR tube containing 3 µL of ddH_2O, and stored at –20°C until direct PCR.

The small subunit (SSU), the internal transcribed spacers (ITS) including the 5.8S, and the large subunit (LSU, D1+D2 region) of the rRNA operon, were amplified using the primers specified in Nézan et al. (2012). Genomic DNA was amplified in 25 µL PCR reaction

containing either 1 µL of extracted DNA or isolated cells, 6.5 µL of ultrapure water, 2.5 µL of each primer (10 µM), and 12.5 µL of PCR Master Mix 1X (Promega, Madison, WI, USA), which included Taq polymerase, dNTPs, $MgCl_2$, and reaction buffer. PCRs were performed in a Mastercycler Personal (Eppendorf, Hamburg, Germany) as follows: one initial denaturation step at 94°C for 2 min, followed by 45 cycles each consisting of 94°C for 30s, 52°C for 1 min, and 72°C for 4 min, and a final elongation at 72°C for 5 min. To obtain at least two sequences of each locus and each strain, cloning was performed if applicable. Then, PCR products were cloned in the pGEM®-T Easy Vector System I (Promega, Madison, WI, USA), visualized, purified, and sequenced following standard protocols (Nézan et al. 2012). At least three positive clones were sequenced in both directions.

In total, 45 new sequences were generated in the course of the present study (Tab. 1). The taxon sample covered the known molecular and morphological diversity of the Amphidomataceae (43 operational taxonomic units: OTUs corresponding to eleven species currently recognized), including 15 OTUs of the three new species. All members of the Gymnodiniaceae, Kareniaceae, Peridiniaceae, and Thoracosphaeraceae exhibiting complete SSU+ITS+LSU sequences (with branches of comparable length in molecular trees: Gu et al. 2013a) were used as outgroup (Tab. S1). The data set was partitioned into four parts (i.e., SSU, ITS, LSU ≤D2, LSU ≥D3), and the nucleotide sequences were separately aligned using MAFFT v6.624b (Katoh et al., 2005; freely available at http://align.bmr.kyushuu.ac.jp/mafft/software/) with the --auto option and considering the secondary structure of the molecules (i.e., the 'QINSI' option). The sequences were concatenated afterwards, and the final data matrix is available as NEXUS file upon request.

Phylogenetic analyses of concatenated sequences were carried out using the resources available from the CIPRES Science Gateway (Miller et al., 2010) with maximum likelihood (ML) and Bayesian inference methods. For ML calculations, RAxML v7.2.6 (Stamatakis, 2006; freely available at http://wwwkramer.in.tum.de/exelixis/software.html) was applied. To

determine best fitted ML-trees, we executed 10-tree searches from distinct random stepwise addition sequence maximum parsimony starting trees and 1,000 non-parametric bootstrap replicates. Bayesian analyses was performed using MrBayes v3.1.2 (Ronquist and Huelsenbeck, 2003; freely available at http://mrbayes.csit.fsu.edu/download.php), under the random-addition-sequence method with 10 replicates and the same GTR+Γ model available in RAxML. We ran two independent analyses of four chains (one cold and three heated) under the partition data mode with 15,000,000 cycles, sampled every 1,000th cycle, with an appropriate burn-in (10%) as inferred from the evaluation of the trace files using Tracer v1.5 (http://tree.bio.ed.ac.uk/software/tracer/). Statistical support values (LBS: ML bootstrap support, BPP: Bayesian posterior probabilities) were drawn on the resulting, best-scoring ML tree.

Acknowledgments

Thanks to Captain Bergmann and the FS Maria S. Merian crew for their assistance and support for the collection of field material. Financial support was provided by the PACES research program of the Alfred Wegener Institute as part of the Helmholtz Foundation initiative in Earth and Environment. This work is part of the project ‘‘Azaspiracids: Toxicological Evaluation, Test Methods and Identification of the Source Organism’’ [PBA/AF/08/001(01)], which is carried out under the Sea Change strategy with the support of the Marine Institute and the Marine Research Sub-Programme of the National Development Plan 2007–2013, co-financed under the European Regional Development Fund. We are grateful to Karine Chèze (MNHN, Concarneau) for her contribution to sequencing.

1 Table 1: Overview of *Azadinium* strains analyzed in the present study.

strain	species	isolated from station nr.	AZA toxins	Fragment Sequence	Molecular Method	Accession nr.
A2D11	*Azadinium trinitatum*	540	negative	ITS-LSU(D1-D3)	DNA extract	KJ481804
				ITS	DNA extract	KJ481806
				LSU (D1-D3)	cloning (clone2)	KJ481814
				LSU (D1-D3)	cloning (clone5)	KJ481805
				LSU (D1-D3)	cloning (clone9)	KJ481807
				SSU	DNA extract	KJ481813
				SSU	DNA extract	KJ481803
4A8	*Azadinium trinitatum*	537	negative	ITS-LSU(D1-D3)	DNA extract	KJ481812
				ITS	DNA extract	KJ481809
				LSU (D1-D3)	DNA extract	KJ481810
				SSU	DNA extract	KJ481808
				SSU	DNA extract	KJ481811
4B11	*Azadinium trinitatum*	537	negative	ITS-LSU(D1-D3)	DNA extract	KJ481816
				ITS-LSU(D1-D3)	DNA extract	KJ481818
				SSU	DNA extract	KJ481815
				SSU	DNA extract	KJ481817
3D6	*Azadinium cuneatum*	532	negative	ITS-LSU(D1-D3)	DNA extract	KJ481820
				ITS-LSU(D1-D3)	DNA extract	KJ481823
				LSU (D1-D3)	cloning (clone 1)	KJ481824
				LSU (D1-D3)	cloning (clone 6)	KJ481825
				LSU (D1-D3)	cloning (clone 10)	KJ481821
				SSU	DNA extract	KJ481819
				SSU	DNA extract	KJ481822
1C6	*Azadinium concinnum*	525	negative	ITS-LSU(D1-D3)	Single cell	KJ481830
				ITS	DNA extract	KJ481827
				LSU (D1-D3)	cloning (clone 4)	KJ481831
				LSU (D1-D3)	cloning (clone 5)	KJ481832
				LSU (D1-D3)	cloning (clone 6)	KJ481833
				SSU	Single cell	KJ481826
				SSU	Single cell	KJ481829

2

3

1 Table 2: Mass transitions m/z (Q1>Q3 mass) and their respective AZAs

Mass transition	AZA	Collision energy (CE) [V]
716>698	AZA-33	40
816>798	AZA-34, AZA-39	40
816>348	AZA-39	70
828>810	AZA-3	40
828>658	AZA-3	70
830>812	AZA-35, AZA-38	40
830>348	AZA-38	70
842>824	AZA-1, AZA-6, AZA-40	40
842>672	AZA-1	70
842>348	AZA-40	70
844>826	AZA-4, AZA-5	40
846>828	AZA-37	40
846>348	AZA-37	70
854>846	AZA-41	40
854>670	AZA-41	70
856>838	AZA-2	40
856>672	AZA-2	70
858>840	AZA-7, AZA-8, AZA-9, AZA-10, AZA-36	40
858>348	AZA-36	70
860>842	Undescribed	40
872>854	AZA-11, AZA-12	40

2

Tab. 3: Compilation of morphological features of all species of *Azadinium* and of the related species *Amphidoma languida*

	A. spinosum	*A. obesum*	*A. poporum*	*A. caudatum* var. *margalefii*	*A. caudatum* var. *caudatum*	*A. polongum*	*A. dexteroporum*	*A. dalianense*	*A. trinitatum*	*A. cuneatum*	*A. concinnum*	*Amphidoma languida*
Length range (mean)	12.3-15.7 (13.8)	13.3-17.7 (15.3)	11.3-16.3 (13.0)	25.0-42.1	35.5-52.5	10.1-17.4 (13.0)	7.0-10.0 (8.5)	11.9-18.0 (13.9)	11.5-16.7 (14.1)	11.2-16.9 (14.2)	8.0-11.5 (9.5)	12.9-15.5 (13.9)
Width range (mean)	7.4-10.3 (8.8)	10.0-14.3 (11.7)	8.0-11.6 (9.8)	18.4-30.0	25.0-36.7	7.4-13.6 (9.7)	5.0-8.0 (6.2)	8.3-12.7 (10.1)	7.3-11.5 (9.2)	8.3-12.7 (10.8)	5.6-8.3 (6.6)	9.7-14.1 (11.9)
L/W ratio	1.6	1.3	1.3	1.2	1.2	1.3	1.4	1.4	1.5	1.3	1.4	1.3
Number apical / intercalary plates	4 / 3	4 / 3	4 / 3	4 / 3	4 / 3	4 / 3	4 / 3	3 / 2	4 / 3	4 / 3	4 / 3	6 / 0
Antapical spine	spine	No	no	short horn, long spine	long horn, short spine	spine	spine	rare, short spine	spine, (unstable?)	no	spine	no
Stalked pyrenoid	1	none	up to four	none	not shown	none	1	up to two	1 (up to two)	1 (up to two)	none	1
1´´ adjacent to 1a	yes	no	yes	yes	yes	yes	yes	yes	yes	no	no	not applicable
Vp position	left side of 1´	left side of 1´	pore plate, left side	pore plate, right side	right side of 1´	left side of 1´	end of pore plate, right side	pore plate, left side	end of pore plate, left side	middle of pore plate, left side	pore plate, right side	right side of 1´ (anterior position)
Pore plate symmetry	suture to 1´slightly asymmetric, right side more apical	suture to 1´slightly asymmetric, right side more apical	suture to 1´ slightly asymmetric., left side more apical	suture to 1´almost symmetric	suture to 1´almost symmetric	Po elongated, suture to 1´almost symmetric	suture to 1´ strongly asymmetric, left side more apical	suture to 1´almost symmetric	suture to 1´ asymmetric, right side more apical	suture to 1´strongly asymmetric, left side more apical	suture to 1´almost symmetric	suture to 1´almost symmetric
Shape of 1´plate	wide posteriorly	narrow posteriorly	wide posteriorly	narrow posteriorly	narrow posteriorly	wide post., narrowed anteriorly	narrow posteriorly	wide posteriorly	narrow posteriorly	wide posteriorly, anteriorly copped	narrow posteriorly	narrow posteriorly
Rel. size first and last intercalary	large	small	large	small	small	small	small	large	large	large	small	not applicable
Relative size apical plates	medium	medium	medium	medium	medium	medium	small	medium	small	large	small	small
AZAs	AZA-1, -2, -716	none	Aza-2, -846, -872, none (strain specific)	none	not tested	none	Aza-3, -7; none (strain specific)	none	none	none	none	AZA-816, -830
Records	North Sea, Atlantic, Pacific off Mexico	North Sea	North Sea, Asia Pacific	Mediterranean, North Sea, Atlantic	Mediterranean, North Sea, Atlantic	North Sea	Mediterranean, North Atlantic	Asian Pacific	North Atlantic	North Atlantic	North Atlantic	North Atlantic
Reference	a, b, c	d	e, f, g, h	i, j	i	k	l, m	n	o	o	o	p, h, m

References : [a)] Tillmann et al. 2009 ; [b)] Salas et al. 2012 ; [c)] Tillmann et al. 2012b ; [d)] Tillmann et al 2010 ; [e)] Tillmann et al. 2011 ; [f)] Potvin et al. 2012 ; [g)] Gu et al. 2013 ; [h)] Krock et al. 2012 ; [i)] Nézan et al. 2012 ; [j)] Tillmann et al. 2014b ; [k)] Tillmann et al. 2012b ; [l)] Percopo et al. 2013 ; [m)] Tillmann et al. (unpublished); [n)] Luo et al. 2013; [o)] This study; [p)] Tillmann et al. 2012a

Figure legends

Fig. 1: Geographical locations of selected sampling stations of the "Maria S. Merian" expedition 2012.

Fig. 2: *Azadinium trinitatum* (strain 4A8). Light microscopy of formalin fixed cells except for E (Lugol fixed). (A-C) General size and shape. Note the presence of a large pyrenoid in the episome and the presence of an antapical spine (arrow in B and C). (D) Lateral view to illustrate a ribbon-like connection of the parietally located chloroplast from epi- to the hyposome. (E) Cell with a purple stained pyrenoid and additional large grains of presumably storage material. (F-G) Variations in pyrenoid, a cell with a large and unusually shaped pyrenoid (F) and a cell with two pyrenoids (G). (H-K) Formalin fixed cell stained with DAPI as viewed using UV excitation showing nucleus and chloroplast shape and position. (L) A cell with UV excitation after calcofluor staining showing a dorsal view of the thecal plates. Scale bars = 2 µm.

Fig. 3: *Azadinium trinitatum*: SEM micrographs of different thecate cells (A: strain 4B11; all others: strain A2D11). (A-C) Ventral view. (D) Dorsal view. Scale bars = 2 µm.

Fig. 4: *Azadinium trinitatum*. Schematic illustration of thecal plates (as inferred from the investigation of strain A2D11). (A) ventral view. (B) Dorsal view. (C) Apical view. (D) Antapical view. Abbreviations: Sa, Sd, Sm, Sp, Ss: sulcal plates as detailed in Fig.6. Arrows in C-D indicate plate overlap pattern.

Fig. 5: *Azadinium trinitatum*: SEM micrographs of different cells (A, D, F, H: strain 4B11; B, G: strain 4A8; C, E, I: strain A2D11). (A, B) Apical view showing the complete series of epithecal plates. Black arrows in (B) exemplarily indicate postion of differently sized

pores on the thecal plates. (C-F) Epitheca in ventral (C), dorsal (D), left lateral (E) or right lateral (F) view. (G-I) Details of the apical pore complex (APC). (G, H) APC in apical view. (I) APC viewed interiorly of the cell. Po = pore plate, vp = ventral pore (arrow); x = X-plate, cp =cover plate. Scale bars = 2 µm (A-F) or = 0.5 µm (G-I).

Fig. 6: *Azadinium trinitatum*: SEM micrographs of different cells (A, D: strain 4A8; B, C: strain 4B11; E, F: strain A2D11). (A, B) Antapical view of hypothecal plates. Black arrows exemplarily indicate position of pores on the thecal plates. (C) Ventral view of cingulum and hypotheca. (D) Dorsal/apical view of the hypotheca showing the series of cingular plates with an interior view of the sulcal plates. (E, F) Details of the sulcal plate arrangement in external (E) and interior (F) view. Black arrows indicate the position of a row of pores on the Sa plate and of a cluster of pores on the C1 plate. (Sa: anterior sulcal plate; Sp: posterior sulcal plate; Ss: left sulcal plate; Sm: median sulcal plate; Sd: right sulcal plate). Scale bars = 2 µm.

Fig. 7: *Azadinium cuneatum* (strain 3D6): LM of living (B, C) or formalin fixed (all other) cells. (A-C) General size and shape. Note the noticeable apical pore complex (arrow in B). (D) Dorsal view of the episome. Note the large pyrenoid and the parietal chloroplast. (E-F) Variation in pyrenoid, which rarely could be located in the hyposome (E), or two pyrenoids present in the episome (F). (G-H) Same cell stained with DAPI in bright (G) or with UV excitation (H) to indicate shape and location of the nucleus. (I-K) Different views of the same DAPI stained cell in brightfield (I), with UV excitation (J), or with blue light excitation (K) to show shape and location of the nucleus and of the chloroplast. Scale bars = 2 µm.

Fig. 8: *Azadinium cuneatum* (strain 3D6): SEM micrographs of different thecate cells. (A-B) Ventral view. (C) Left lateral view. (D) Dorsal view. Black arrows exemplarily indicate the position of pores on the thecal plates. Scale bars = 2 µm.

Fig. 9: *Azadinium cuneatum*: Schematic illustration of thecal plates (as inferred from the investigation of strain 3D6). (A) ventral view. (B) Dorsal view. (C) Apical view. (D) Antapical view. Abbreviations: Sa, Sd, Sm, Sp, Ss: sulcal plates as detailed in Fig. 12. Arrows in C-D indicate plate overlap pattern.

Fig. 10: *Azadinium cuneatum* (strain 3D6): SEM micrographs of different cells to illustrate epithecal plate arrangement. (A) Apical view (B) Ventral/apical view. (C) Left lateral view (D) ventral view. (E-F) Dorsal view. Note the tetragonal shape of the median intercalary plate 2a in (E) and a more rarely found pentagonal configuration of plate 2a in (F). Black arrows in (E) exemplarily indicate the position of pores on the precingular plates. Scale bars = 2 µm.

Fig. 11: *Azadinium cuneatum* (strain 3D6): Details of the apical pore complex (APC). (A-E) External view of APC in apical view. Note the rare case in (E), where the rim around Po is extending along the suture of plate 1´ and 2´ (arrow). (F) APC viewed interiorly from the cell. Po = pore plate, vp = ventral pore (arrow); x = X-plate, cp = cover plate. Scale bars = 0.5 µm.

Fig. 12: *Azadinium cuneatum* (strain 3D6): SEM micrographs of different cells. (A, B) Antapical view of hypothecal plates. Black arrows in (A) exemplarily indicate the position of pores on the postcingular plates. (C) Dorsal/apical view of the hypotheca showing the series of cingular plates (C) with an interior view of the sulcal plates. (D)

Details of the sulcal plate arrangement in external view. (E) Details of the sulcal plate arrangement in interior view. (Sa: anterior sulcal plate; Sp: posterior sulcal plate; Ss: left sulcal plate; Sm: median sulcal plate; Sd: right sulcal plate). Scale bars = 2 µm.

Fig. 13: *Azadinium concinnum* (strain 1C6): LM of formalin fixed cells. (A-E) General size and shape. Note the prominent apical pore complex (black arrow in B), the very prominent antapical spine (white arrow in C), and the spherical bodies of varying size in both the epi- and hyposome (D, E). (F-I) Pair of same DAPI stained cells in either bright-field (F, H) or with UV excitation (G, I) to indicate shape and position of nucleus and chloroplast. Scale bars = 2 µm.

Fig. 14: *Azadinium concinnum* (strain 1C6): SEM micrographs of different thecate cells. (A-B) Ventral view. (B) Dorsal view. Black arrows exemplarily indicate positions of pores on the thecal plates. Scale bars = 2 µm.

Fig. 15: *Azadinium concinnum*: Schematic illustration of thecal plates (as inferred from the investigation of strain 1C6). (A) ventral view. (B) Dorsal view. (C) Apical view. (D) Antapical view. Abbreviations: Sa, Sd, Sm, Sp, Ss: sulcal plates as detailed in Fig. 17. Arrows in C-D indicate plate overlap pattern.

Fig. 16: *Azadinium concinnum* (strain 1C6): SEM micrographs of different cells to illustrate epithecal plate arrangement and the apical pore complex (APC). (A) Apical view. Note a vertical row of pores on the first apical plate. (B) Ventral/apical view. (C) Left lateral view (D) Dorsal view. Black arrows indicate position of pores on the intercalary plates. (E) Right lateral view. (F-G) Ventral view of the APC. Black arrow in (G) indicate the position of a row or pores on the first apical plate. (H) External view of APC in apical

view. (I) APC interiorly viewed from the cell. Po = pore plate, vp = ventral pore (arrow); X = X-plate, cp = cover plate. Scale bars = 1 µm (A-E) or = 0.5 µm (F-I).

Fig. 17: *Azadinium concinnum* (strain 1C6): SEM micrographs of different cells. (A) Antapical view of hypothecal plates. Note conspicuous pores near the sutures of postcingular plates (black arrows). (B-C) Ventral/antapical view of cingulum and hypotheca. (D) Detailed view of sulcal plates. (E) Dorsal/apical view of the hypotheca showing the series of cingular plates. (Sa: anterior sulcal plate; Sp: posterior sulcal plate; Ss: left sulcal plate; Sm: median sulcal plate; Sd: right sulcal plate). Scale bars = 1 µm.

Fig. 18: Maximum likelihood tree (–ln = 72424.15) of 43 OTU assigned to the Amphidomataceae, as inferred from a MAFFT generated rRNA nucleotide alignment spanning the SSU, ITS and LSU (1813 parsimony-informative positions). Major clades are indicated, and branch lengths are drawn to scale, with the scale bar indicating the number of nucleotide substitutions per site. Numbers on branches are statistical support values for the clusters to the right of them (above: ML bootstrap support values, values under 50 are not shown; below: Bayesian posterior probabilities, values under .90 are not shown), and asterisks indicate maximal support values. The tree is rooted with 88 of the Gymnodiniaceae, Kareniaceae, Peridiniaceae, and Thoracosphaeraceae.

Fig. 19: Comparison of APC of *A. poporum* (A) and *A. trinitatum* (B). Scale bars = 0.5 µm.

Fig. 20: Potential transition between apical plate pattern of *Azadinium* (A: interpretative for *A. concinnum*) and *Amphidoma* (B: interpretative for *A. languida*). When the dorsal apical plate 3´ of *Azadinium* is lost (C), all three intercalary plate may get in contact to the pore

plate leading to an "*Amphidoma*" arrangement (D). Alternatively, when the medium intercalary plate of *Azadinium* is lost (E), the two remaining intercalary plates may get in contact to the pore plate leading to an "*Amphidoma*" configuration (F).

References

Akselman R, Negri A (2012) Blooms of *Azadinium* cf. *spinosum* Elbrächter et Tillmann (Dinophyceae) in northern shelf waters of Argentina, Southwestern Atlantic. Harmful Algae **19:** 30-38

Auinger BM, Pfandl K, Boenigk J (2008) Improved methodology for identification of protists and microalgae from plankton samples preserved in Lugol's iodine solution: combining microscopic analysis with single-cell PCR. Appl Environ Microbiol **74:** 2505-2510

Bérard-Therriault L, Poulin M, Bossé L (1999) Guide d´identification du phytoplancton marin de l´estuaire et du golfe de Saint-Laurent incluant également certaines protozoaires. Publication spéciale canadienne des sciences halieutiques et aquatiques **128:** 1-387

Braña Magdalena A, Lehane M, Krys S, Fernández ML, Furey A, James KJ (2003) The first identification of azaspiracids in shellfish from France and Spain. Toxicon **42:** 105-108

Dodge JD (1989) Some revisions of the family Gonyaulacaceae (Dinophyceae) based on a scanning electron microscopy study. Bot Mar **32:** 275-298

Dodge JD, Saunders RD (1985) A SEM study of *Amphidoma nucula* (Dinophyceae) and description of the thecal plates in *A. caudata*. Arch Protistenkd **129:** 89-99

Doyle JJ, Doyle JL (1987) A rapid DNA isolation procedure for small quantities of fresh leaf tissue. Phytochem Bull **19:** 11-15

Fritz L, Triemer RE (1985) A rapid simple technique utilizing Calcofluor white M2R for the visualization of dinoflagellate thecal plates. J Phycol **21:** 662-664

Gu H, Kirsch M, Zinßmeister C, Soehner S, Meier KJS, Liu T, Gottschling M (2013a) Waking the dead: Morphological and molecular characterization of extant †*Posoniella tricarinelloides* (Thoracosphaeraceae, Dinophyceae). Protist **164:** 583-597

Gu H, Luo Z, Krock B, Witt M, Tillmann U (2013b) Morphology, phylogeny and azaspiracid profile of *Azadinium poporum* (Dinophyceae) from the China Sea. Hamful Algae **21-22:** 64-75

Hansen G, Moestrup Ø, Roberts KR (1996/97) Light and electron microscopical observations on *Protoceratium reticulatum* (Dinophyceae). Arch Protistenkd **147:** 381-391

Hernández-Becerril DU, Barón-Campis SA, Escobar-Morales S (2012) A new record of *Azadinium spinosum* (Dinoflagellata) from the tropical Mexican Pacific. Revista de Biología Marina y Oceanografía **47:** 553-557

Holmes RW (1956) The annual cycle of phytoplankton in the Labrador Sea, 1950-1951. Bull Bingham Oceanogr Collect **16:** 1-74

James KJ, Furey A, Lehane M, Ramstad H, Aune T, Hovgaard P, Morris P, Higman W, Satake M, Yasumoto T (2002) First evidence of an extensive northern European distribution of azaspirazid poisoning (AZP) toxins in shellfish. Toxicon **40:** 909-915

Jauffrais T, Séchet V, Herrenknecht C, Truquet P, Veronique S, Tillmann U, Hess P (2013) Effect of environmental and nutritional factors on growth and azaspiracid production of the dinoflagellate *Azadinium spinosum* Harmful Algae **27:** 138-148

Keller MD, Selvin RC, Claus W, Guillard RRL (1987) Media for the culture of oceanic ultraphytoplankton. J Phycol **23:** 633-638

Katoh K, Kuma K, Toh H, Miyata T (2005) MAFFT version 5: improved in accuracy of multiple sequence alignment. Nucleic Acids Res **33**: 511–518

Krock B, Tillmann U, Voß D, Koch BP, Salas R, Witt M, Potvin E, Jeong HJ (2012) New azaspiracids in Amphidomataceae (Dinophyceae): proposed structures. Toxicon **60:** 830-839

Krock B, Tillmann U, Witt M, Gu H (2014) Azaspiracid variability of *Azadinium poporum* (Dinophyceae) from the China Sea. Harmful Algae **36**: 22-28

López-Rivera A, O'Callaghan K, Moriarty M, O'Driscoll D, Hamilton B, Lehane M, James KJ, Furey A (2009) First evidence of azaspiracids (AZAs): A family of lipophilic polyether marine toxins in scallops (*Argopecten purpuratus*) and mussels (*Mytilus chilensis*) collected in two regions of Chile. Toxicon **55:** 692-701

Luo Z, Gu H, Krock B, Tillmann U (2013) *Azadinium dalianense*, a new dinoflagellate from the Yellow Sea, China. Phycologia **52:** 625-636

Nézan E, Tillmann U, Bilien G, Boulben S, Chèze K, Zentz F, Salas R, Chomérat N (2012) Taxonomic revision of the dinoflagellate *Amphidoma caudata*: transfer to the genus *Azadinium* (Dinophyceae) and proposal of two varieties, based on morphological and molecular phylogenetic analyses. J Phycol **48:** 925-939

Miller MA, Pfeiffer W, Schwartz T (2010) "Creating the CIPRES Science Gateway for inference of large phylogenetic trees" in Proceedings of the Gateway Computing Environments Workshop (GCE), 14 Nov. 2010, New Orleans, LA 1–8.

Okolodkov YB, Dodge JD (1995) Redescription of the planktonic dinoflagellate *Peridiniella danica* (Paulsen) comb. nov. and its distribution in the N.E. Atlantic. Eur J Phycol **30:** 299-306

Percopo I, Siano R, Rossi R, Soprano V, Sarno D, Zingone A (2013) A new potentially toxic *Azadinium* species (Dinophyceae) from the Mediterranean Sea, *A. dexteroporum* sp. nov. J Phycol **49:** 950-966

Potvin E, Jeong HJ, Kang NST, Tillmann U, Krock B (2012) First report of the photosynthetic dinoflagellate genus *Azadinium* in the Pacific Ocean: Morphology and molecular characterizationof *Azadinium* cf. *poporum*. J Eukaryot Microbiol **59:** 145-156

Poulin M, Daugbjerg N, Gradinger R, Ilyash L, Ratkova T, von Quillefeldt C (2011) The pan-Arctic biodiversity of marine pelagic and sea-ice unicellular eukaryotes: a first-attempt assessment. Mar Biodiv **41:** 13-28

Ramsfjell E (1959) Two new phytoplankton species from the Norwegian Sea, the diatom *Coscinosira poroseriata*, and the dinoflagellate *Gonyaulax parva*. Nytt Mag f Bot **7:** 175-177

Reinecke P (1967) *Gonyaulax grindleyi* sp. nov.: a dinoflagelate causing a red tide at Elands Bay, Cape Province, in december 1966. J S Afr Bot **33:** 157-160

Ronquist F, Huelsenbeck JP (2003) MrBayes 3: Bayesian phylogenetic inference under mixed models. Bioinformatics **19**: 1572–1574

Salas R, Tillmann U, John U, Kilcoyne J, Burson A, Cantwell C, Hess P, Jauffrais T, Silke J (2011) The role of *Azadinium spinosum* (Dinophyceae) in the production of Azasdpiracid Shellfish Poisoning in mussels. Harmful Algae **10:** 774-783

Satake M, Ofuji K, James K, Furey A, Yasumoto T (1998) New toxic events caused by Irish mussels. In Reguera B, Blanco J, Fernandez ML, Wyatt T, (eds) Harmful Algae. Xunta de Galicia and Interantional Oceanographic Commission of UNESCO, Santiago de Compostela, pp 468-469

Schiller J (1935) Dinoflagellatae (Peridineae) in monographischer Behandlung. In Rabenhorst L, (ed) Dr. L. Rabenhorst´s Kryptogamen-Flora von Deutschland, Österreich und der Schweiz. 161-320

Schnepf E, Elbrächter M (1999) Dinophyte chloroplasts and phylogeny - A review. Grana **38:** 81-97

Stamatakis A (2006) RAxML-VI-HPC: Maximum Likelihood- based phylogenetic analyses with thousands of taxa and mixed models. Bioinformatics **22**: 2688–2690

Taleb H, Vale P, Amanhir R, Benhadouch A, Sagou R, Chafik A (2006) First detection of azaspirazids in mussels in north west Africa. J Shellfish Res **25:** 1067-1070

Tillmann U, Elbrächter M (2010) Plate overlap pattern of *Azadinium spinosum* Elbrächter et Tillmann (Dinophyceae), the newly discovered primary source of azaspiracid toxins. In Ho KC, Zhou MJ, Qi YZ, (eds) Proceedings of the 13th International Conference on Harmful Algae. Environmental Publication house, Hong Kong, pp 42-44

Tillmann U, Elbrächter M, John U, Krock B (2011) A new non-toxic species in the dinoflagellate genus *Azadinium*: *A. poporum* sp. nov. Eur J Phycol **46:** 74-87

Tillmann U, Elbrächter M, John U, Krock B, Cembella A (2010) *Azadinium obesum* (Dinophyceae), a new nontoxic species in the genus that can produce azaspiracid toxins. Phycologia **49:** 169-182

Tillmann U, Elbrächter M, Krock B, John U, Cembella A (2009) *Azadinium spinosum* gen. et sp. nov. (Dinophyceae) identified as a primary producer of azaspiracid toxins. Eur J Phycol **44:** 63-79

Tillmann U, Salas R, Gottschling M, Krock B, O´Driscoll D, Elbrächter M (2012a) *Amphidoma languida* sp. nov. (Dinophyceae) reveals a close relationship between *Amphidoma* and *Azadinium*. Protist **163:** 701-719

Tillmann U, Salas R, Jauffrais T, Hess P, Silke J (2014a) Azaspiracids. The Producing Organisms: Biology and Trophic Transfer. In Botana LM, (ed) Seafood and Freshwater Toxins. CRC Press, Boca Raton, USA, pp773-798

Tillmann U, Soehner S, Nézan E, Krock B (2012b) First record of *Azadinium* from the Shetland Islands including the description of *A. polongum* sp. nov. Harmful Algae **20:** 142-155

Tillmann U, Taylor B, Krock B (2014b) *Azadinium caudatum* var. *margalefii*, a poorly known member of the toxigenic genus *Azadinium* (Dinophyceae). Mar Biol Res **10**: 941-956

Toebe K, Joshi AR, Messtorff P, Tillmann U, Cembella A, John U (2013) Molecular discrimination of taxa within the dinoflagellate genus *Azadinium*, the source of azaspiracid toxins. J Plankton Res **35:** 225-230

Wołoszyńska HJ (1928) Dinoflagellatae der polnischen Ostsee sowie der an der Piasnica gelegenen Sümpfe. Archiwum Hydrobiologii i Rybactwa **3:** 155-278

Yao J, Tan Z, Zhou D, Guo M, Xing L, Yang S (2010) Determination of azaspiracid-1 in shellfishes by liquid chromatography with tandem mass spectrometry. Chin J Chrom **28:** 363–367

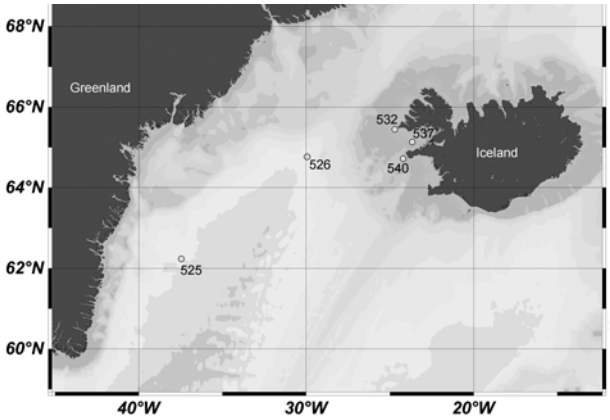
68°N
66°N
64°N
62°N
60°N
40°W
30°W
20°W
Greenland
Iceland
532
537
540
526
525

Fig. 1

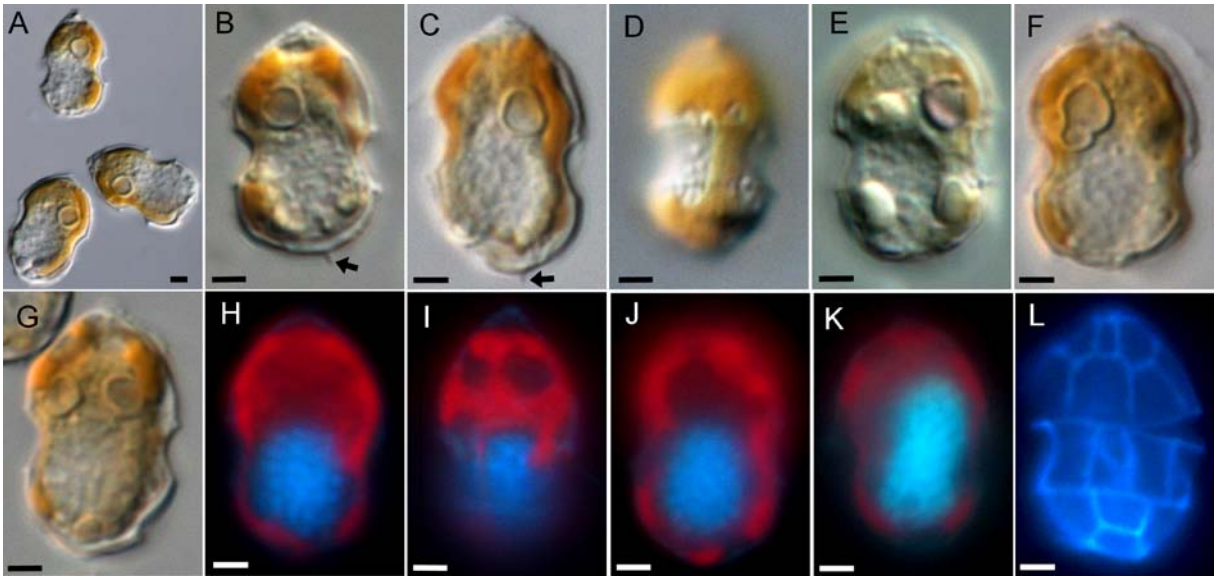

Fig. 2

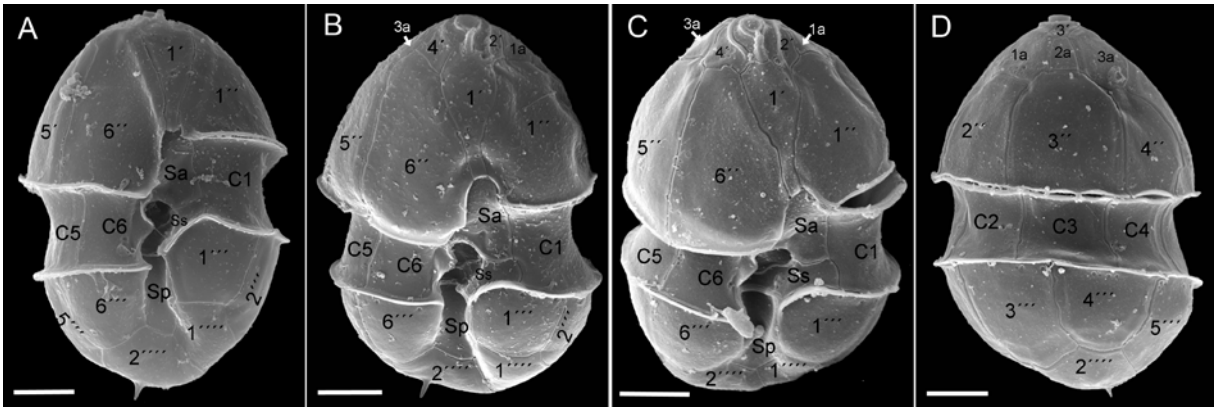
A
1´
1´´
5´
6´´
Sa
C1
C5
C6
Ss
1´´´
Sp
6´´´
2´´´
5´´´´
1´´´´
2´´´´
B
3a
4´
2´
1a
1´
1´´
5´´
6´´
Sa
C5
C6
C1
Ss
6´´´
Sp
1´´´
2´´´
2´´´´
1´´´´
C
3a
4´
2´
1a
1´
1´´
5´´
6´´
Sa
C5
C1
C6
Ss
6´´´
1´´´
Sp
2´´´´
1´´´´
D
3´
1a
2a
3a
2´´
3´´
4´´
C2
C3
C4
3´´´
4´´´
5´´´
2´´´´

Fig. 3

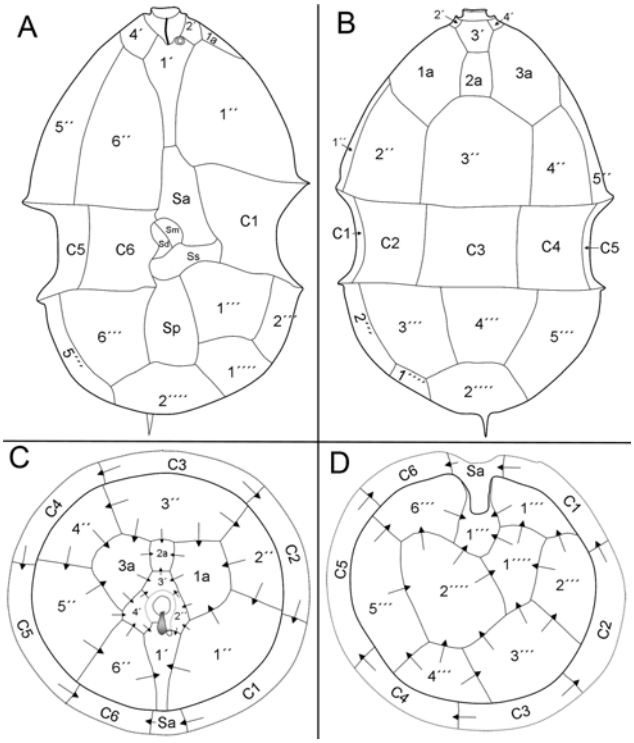

Fig. 4

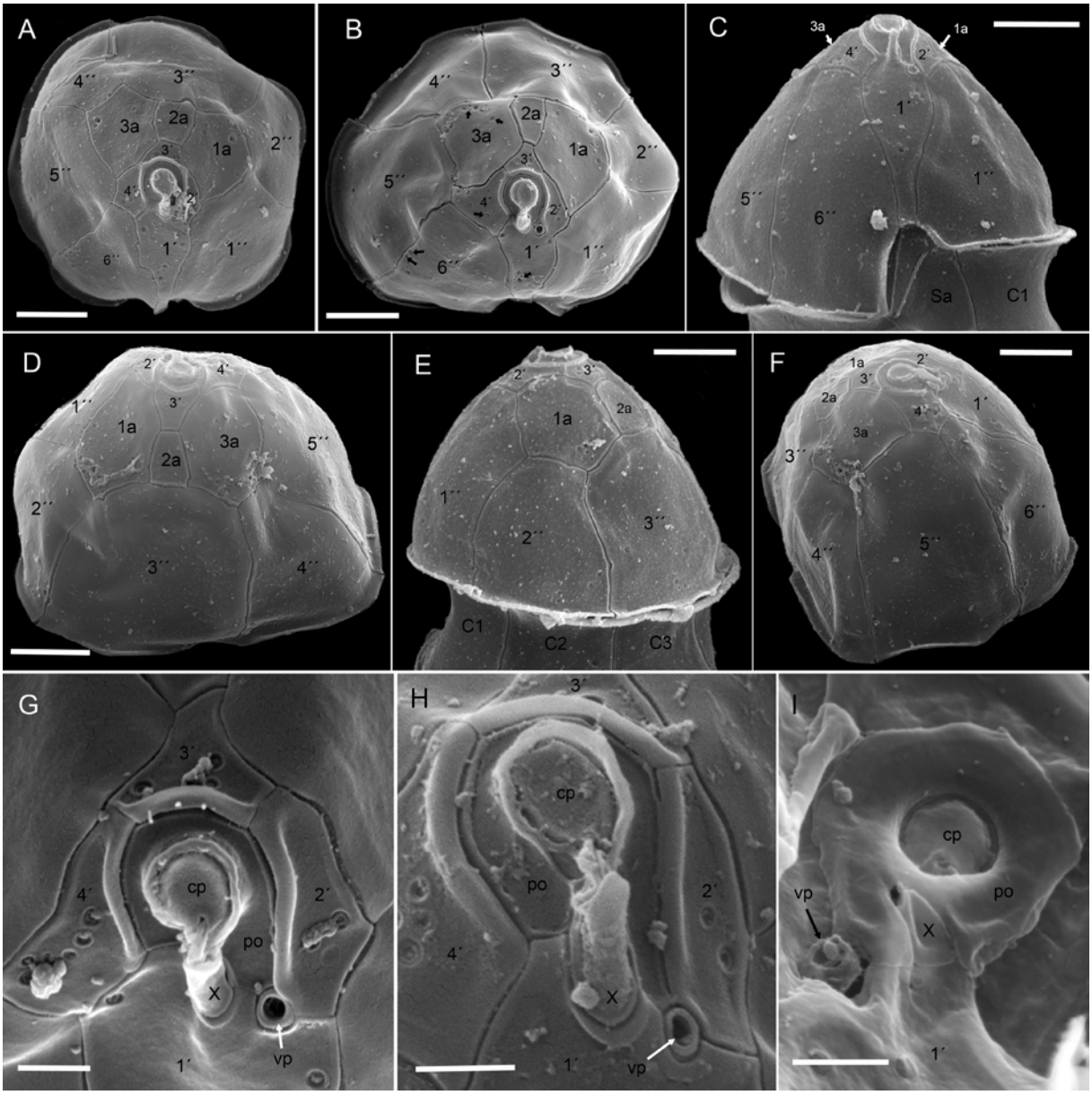
A
4´´
3´´
3a
2a
3´
1a
2´´
5´´
4´
2´
6´´
1´
1´´
B
4´´
3´´
3a
2a
3´
1a
2´´
5´´
4´
2´
6´´
1´
1´´
C
3a
4´
1a
2´
1´´
1´´
5´´
6´´
Sa
C1
D
2´
4´
1´´
3´
1a
3a
5´´
2a
2´´
3´´
4´´
E
2´
3´
1a
2a
1´´
3´´
2´´
C1
C2
C3
F
1a
2´
3´
2a
4´
1´
3a
3´´
6´´
4´´
5´´
G
3´
4´
cp
2´
po
X
1´
vp
H
3´
cp
po
2´
4´
X
1´
vp
I
cp
vp
po
X
1´

Fig. 5

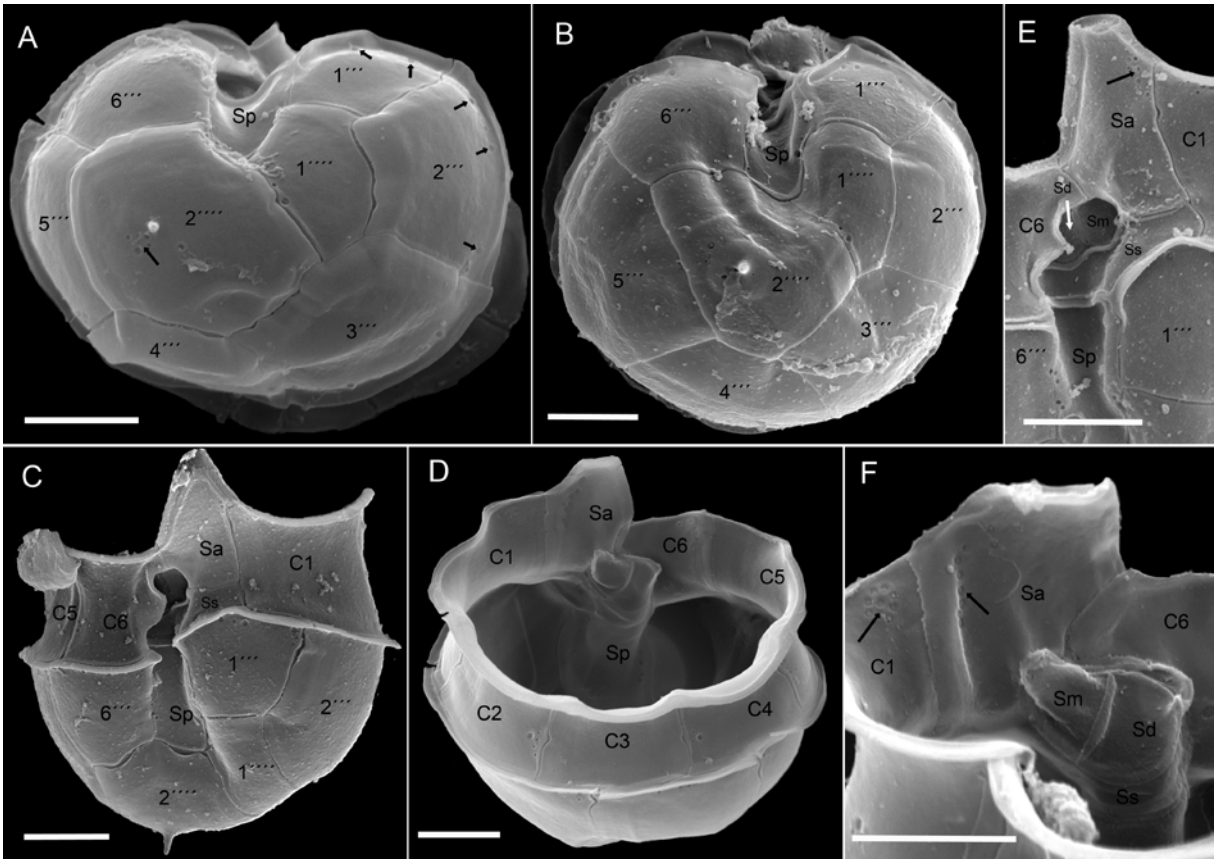
A
6‴
Sp
1‴
1⁗
2‴
5‴
2⁗
4‴
3‴
B
6‴
1‴
Sp
1⁗
2‴
5‴
2⁗
3‴
4‴
E
Sa
C1
Sd
C6
Sm
Ss
1‴
6‴
Sp
C
Sa
C1
C5
C6
Ss
1‴
6‴
Sp
2‴
1⁗
2⁗
D
Sa
C1
C6
C5
Sp
C2
C4
C3
F
Sa
C6
C1
Sm
Sd
Ss

Fig. 6

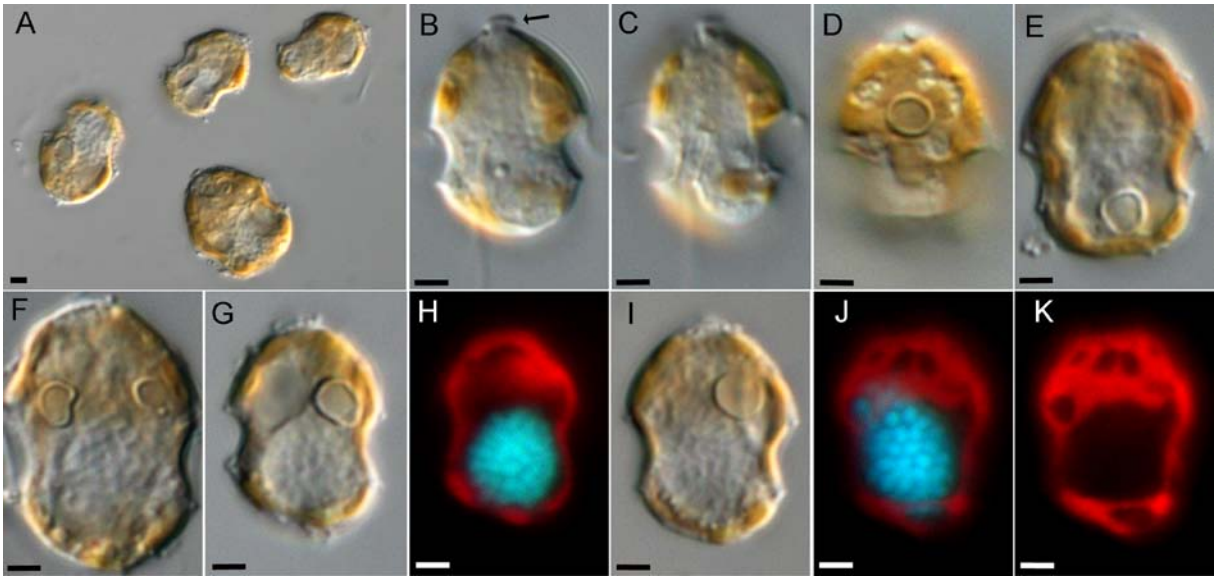

Fig. 7

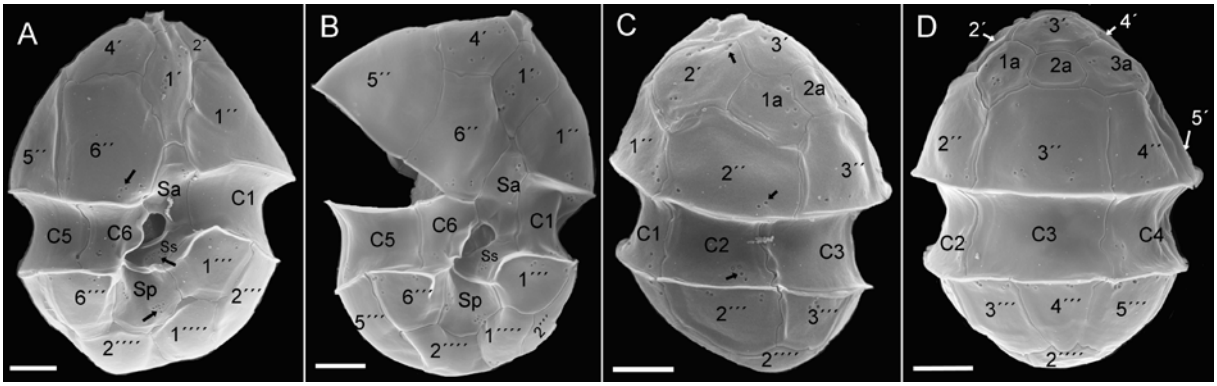
A
4´
2´
1´
1´´
5´´
6´´
Sa
C1
C5
C6
Ss
1´´´
6´´´
Sp
2´´´
2´´´´
1´´´´´
B
4´
5´´
1´
6´´
1´´
Sa
C5
C6
C1
Ss
1´´´
6´´´
Sp
5´´´´
2´´´´
1´´´´
C
3´
2´
1a
2a
1´´
2´´
3´´
C1
C2
C3
2´´´
3´´´
2´´´´
D
2´
3´
4´
1a
2a
3a
5´
2´´
3´´
4´´
C2
C3
C4
3´´´
4´´´
5´´´
2´´´´

Fig. 8

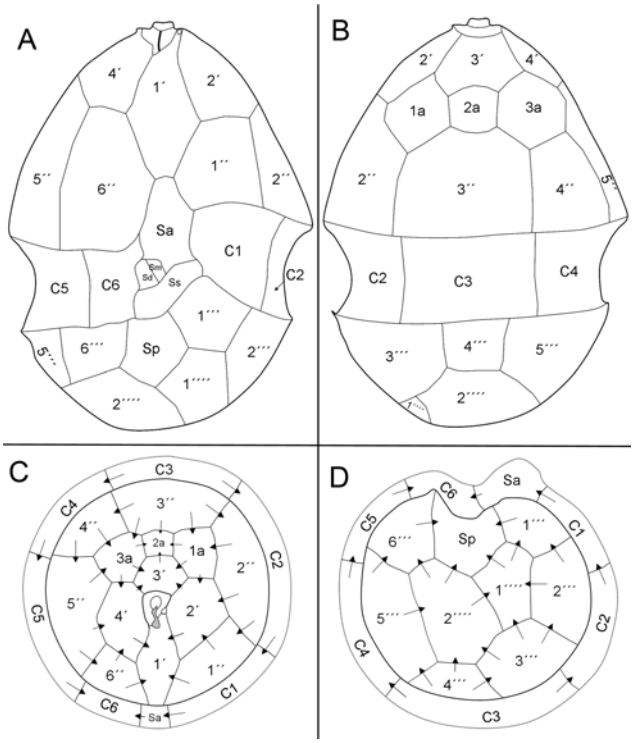
A
4´
1´
2´
5´´
6´´
1´´
2´´
Sa
C1
C2
C5
C6
Sm
Sd
Ss
1´´´
6´´´
Sp
2´´´
5´´´
1´´´´
2´´´´
B
2´
3´
4´
1a
2a
3a
2´´
3´´
4´´
5´´
C2
C3
C4
3´´´
4´´´
5´´´
2´´´´
7´´´´
C
C3
C4
3´´
4´´´
2a
3a
1a
3´
2´´
C2
5´´
4´
2´
C5
6´´
1´
1´´
C6
Sa
C1
D
Sa
C6
C5
6´´´
Sp
1´´´
C1
1´´´´
2´´´
5´´´
2´´´´
C2
C4
3´´´
4´´´
C3

Fig. 9

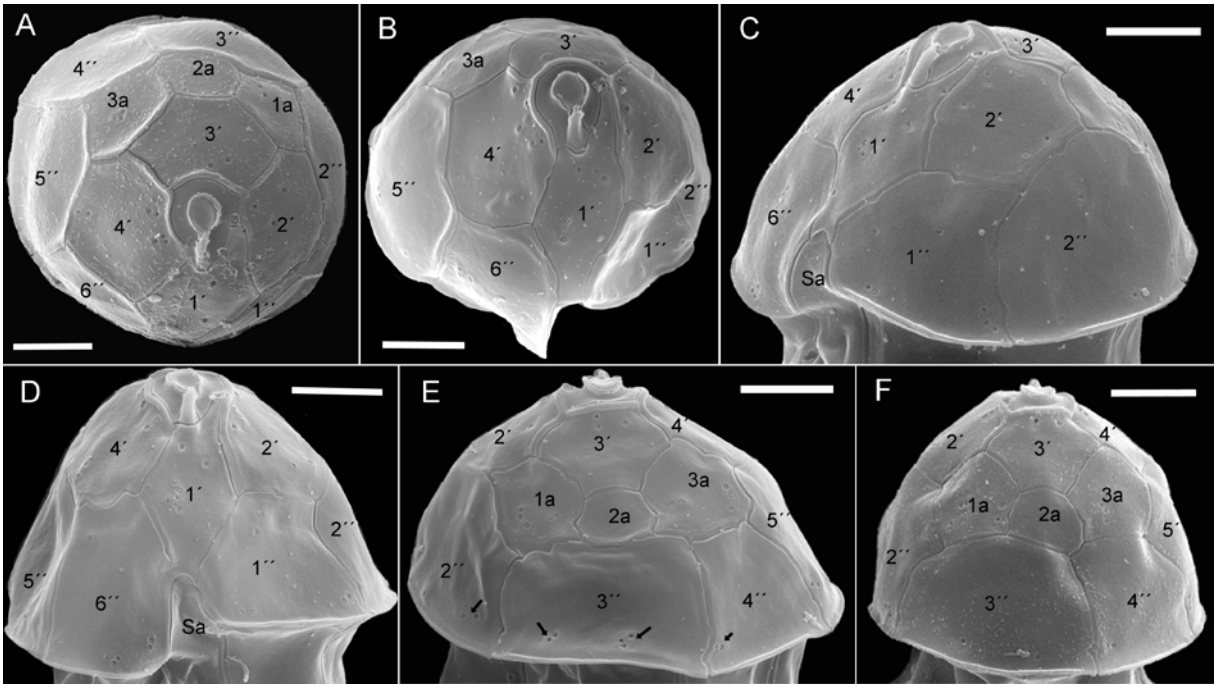
A
3´´
4´´
2a
3a
1a
3´
5´´
2´´
4´
2´
6´´
1´
1´´
B
3´
3a
4´
2´
5´´
2´´
1´
6´´
1´´
C
3´
4´
2´
1´
6´´
1´´
2´´
Sa
D
4´
2´
1´
2´´
5´´
1´´
6´´
Sa
E
2´
3´
4´
3a
1a
2a
5´´
2´´
3´´
4´´
F
2´
3´
4´
1a
2a
3a
5´
2´´
3´´
4´´

Fig. 10

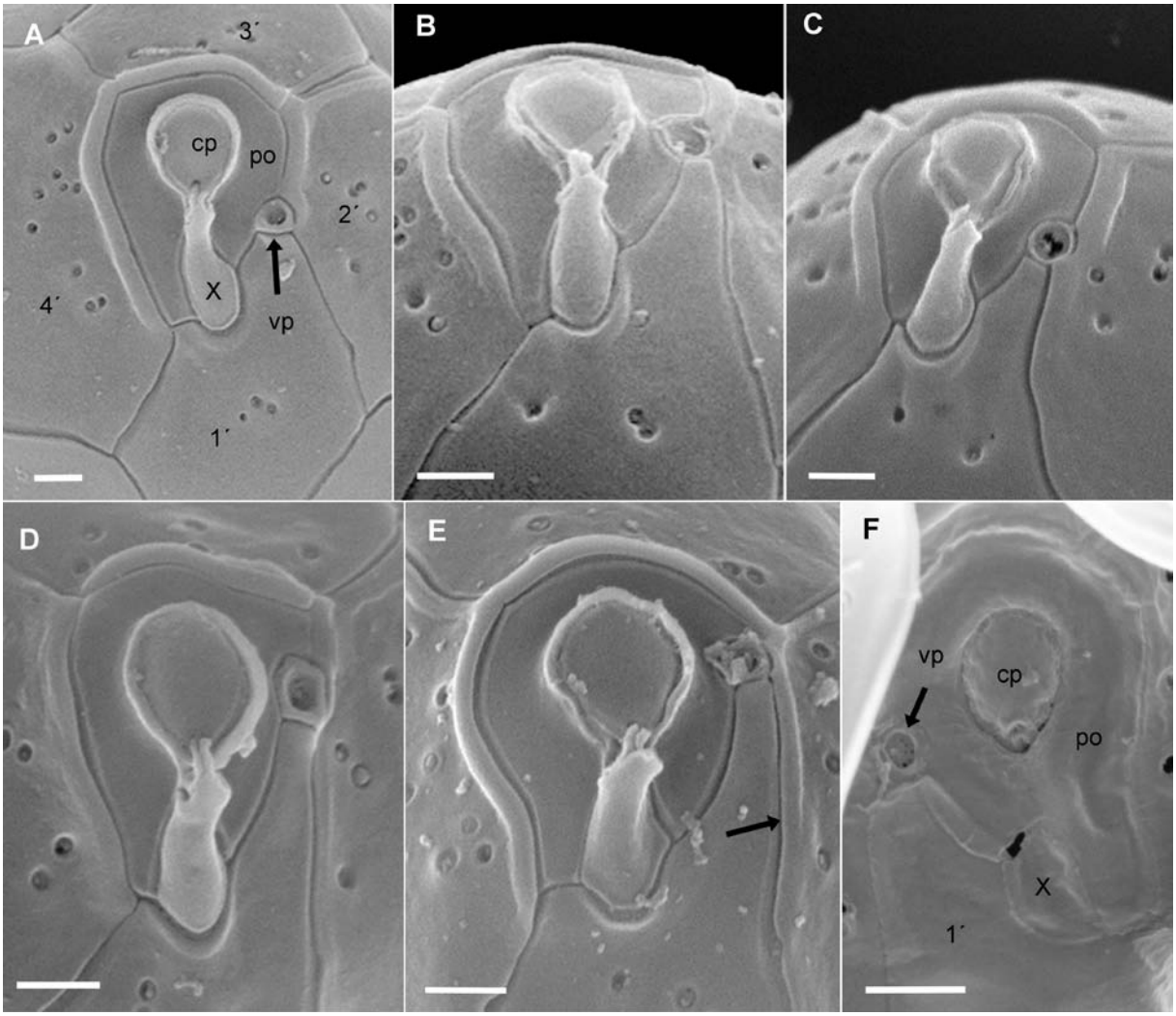

Fig. 11

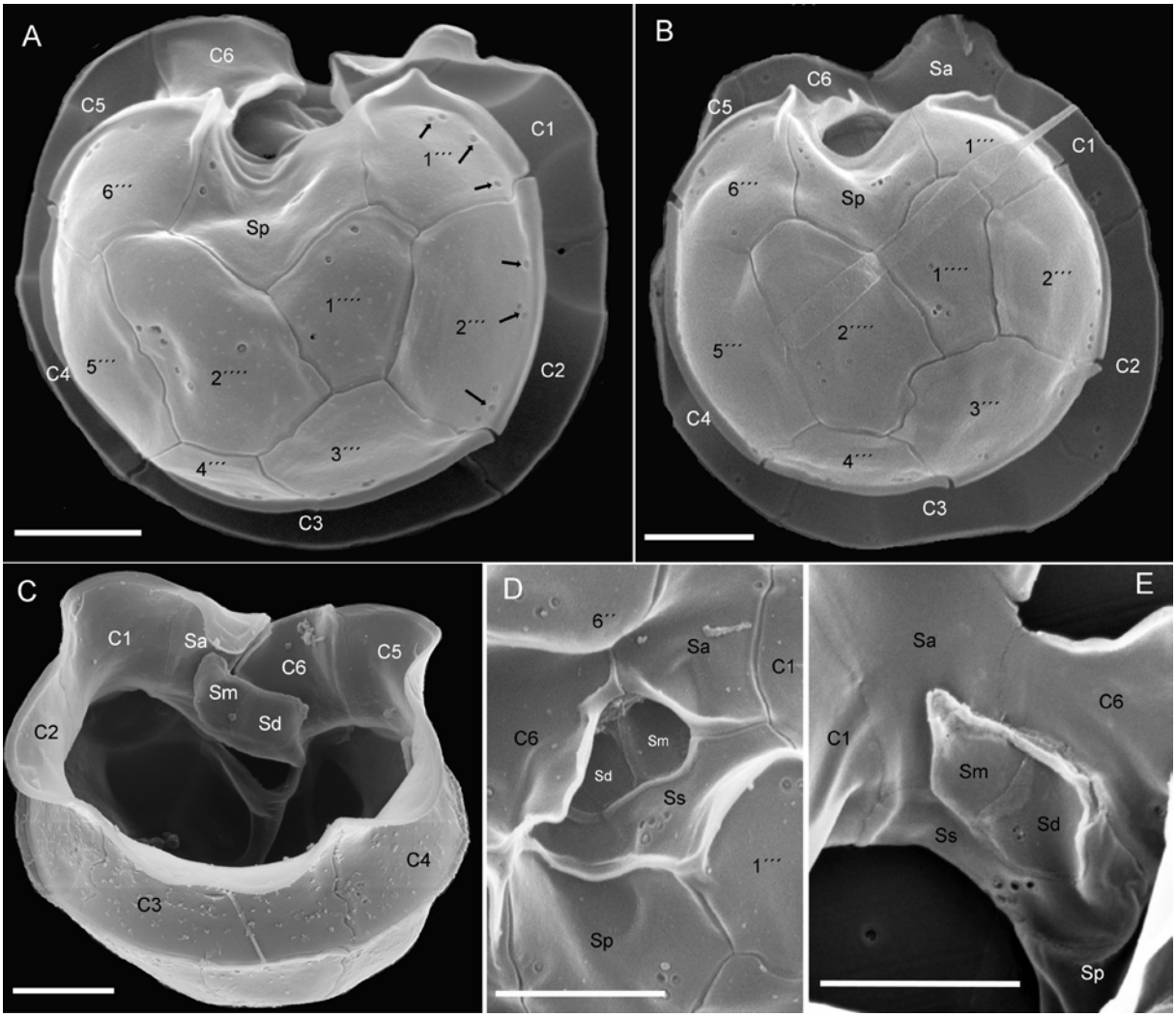
A
C6
C5
C1
1‴
6‴
Sp
1⁗
2‴
2⁗
C4
5⁗
C2
4‴
3‴
C3
B
C6
Sa
C5
1‴
C1
6‴
Sp
1⁗
2‴
2⁗
5‴
C2
3‴
C4
4‴
C3
C
C1
Sa
C6
C5
Sm
Sd
C2
C4
C3
D
6″
Sa
C1
C6
Sm
Sd
Ss
1‴
Sp
E
Sa
C6
C1
Sm
Ss
Sd
Sp

Fig. 12

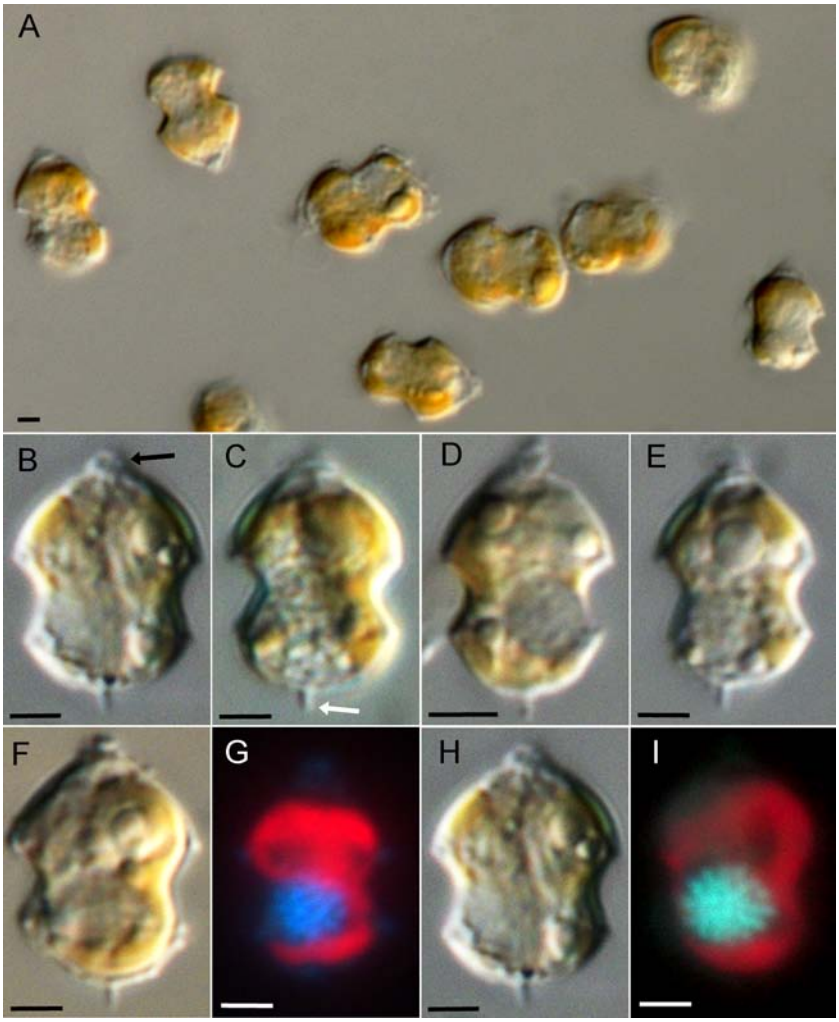

Fig. 13

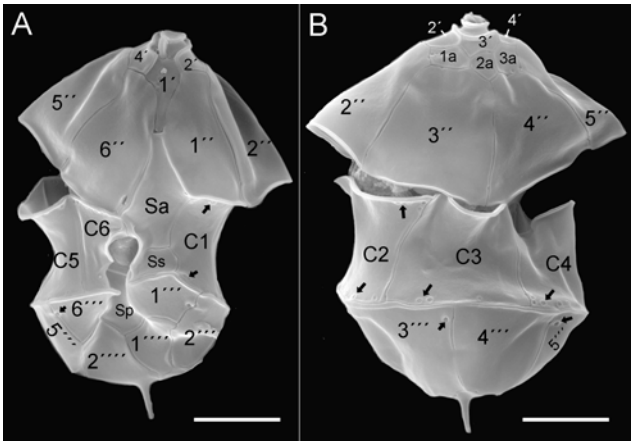

Fig. 14

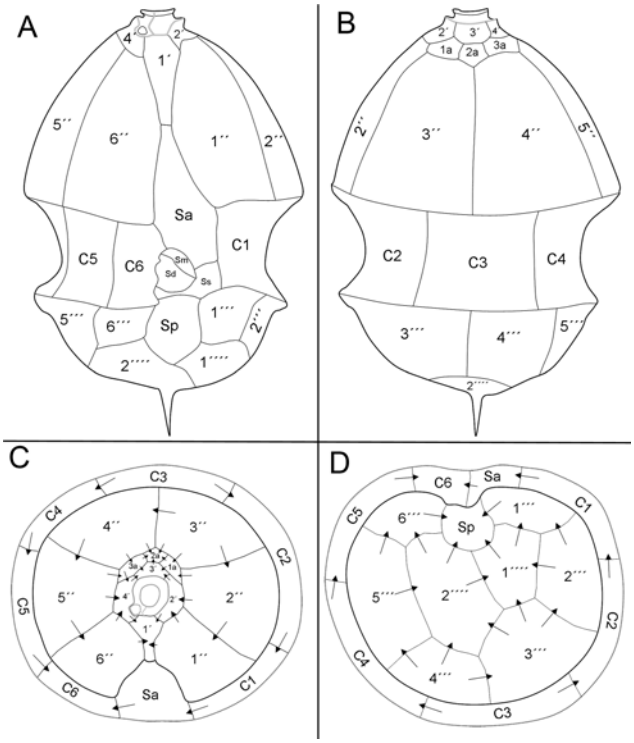

Fig. 15

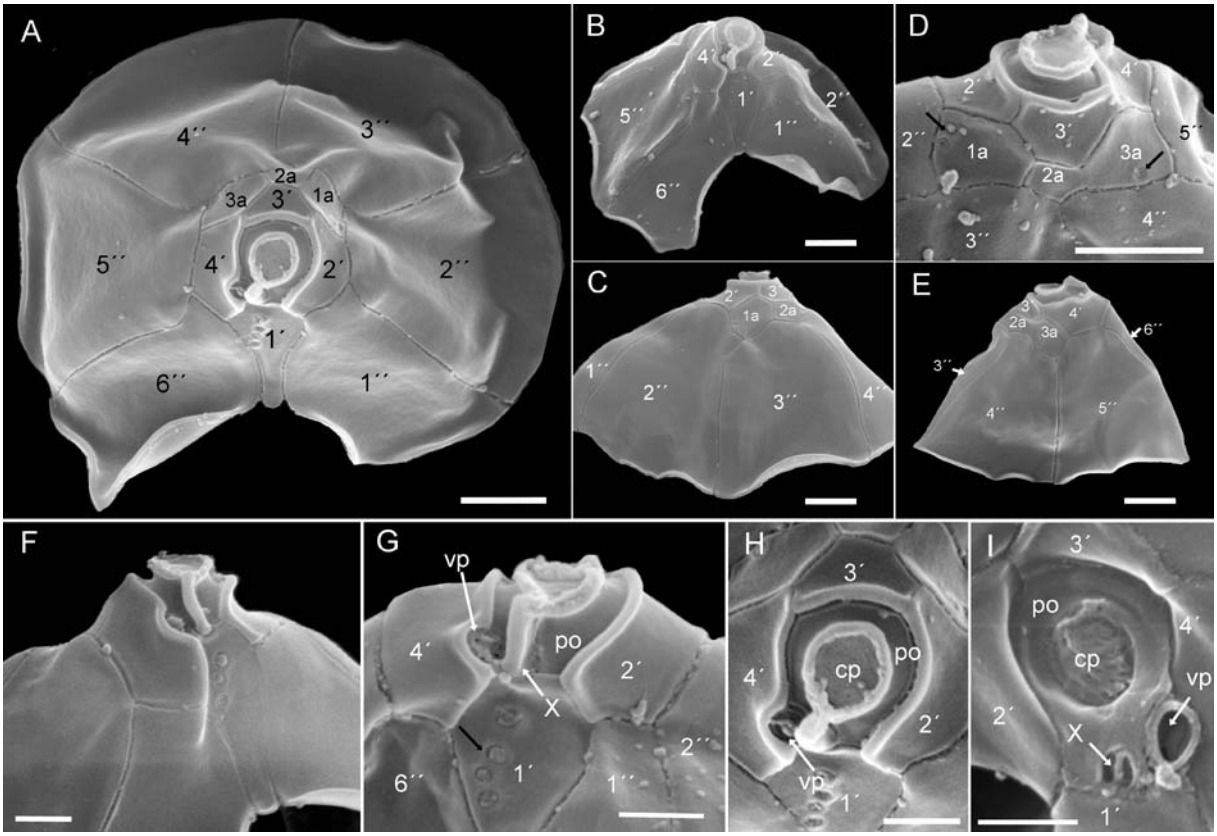
A
4´´
3´´
2a
3a
3´
1a
5´´
4´
2´
2´´
1´
6´´
1´´
B
4´
2´
5´´
1´
2´´
1´´
6´´
C
2´
3
1a
2a
1´´
2´´
3´´
4´
D
2´
4´
2´´
1a
3´
3a
5´´
2a
4´´
3´´
E
3
2a
4´
3a
6´´
3´´
4´´
5´´
F
G
vp
4´
po
2´
X
2´´
6´´
1´
1´´
H
3´
4´
cp
po
2´
vp
1´
I
3´
po
4´
cp
vp
2´
X
1´

Fig. 16

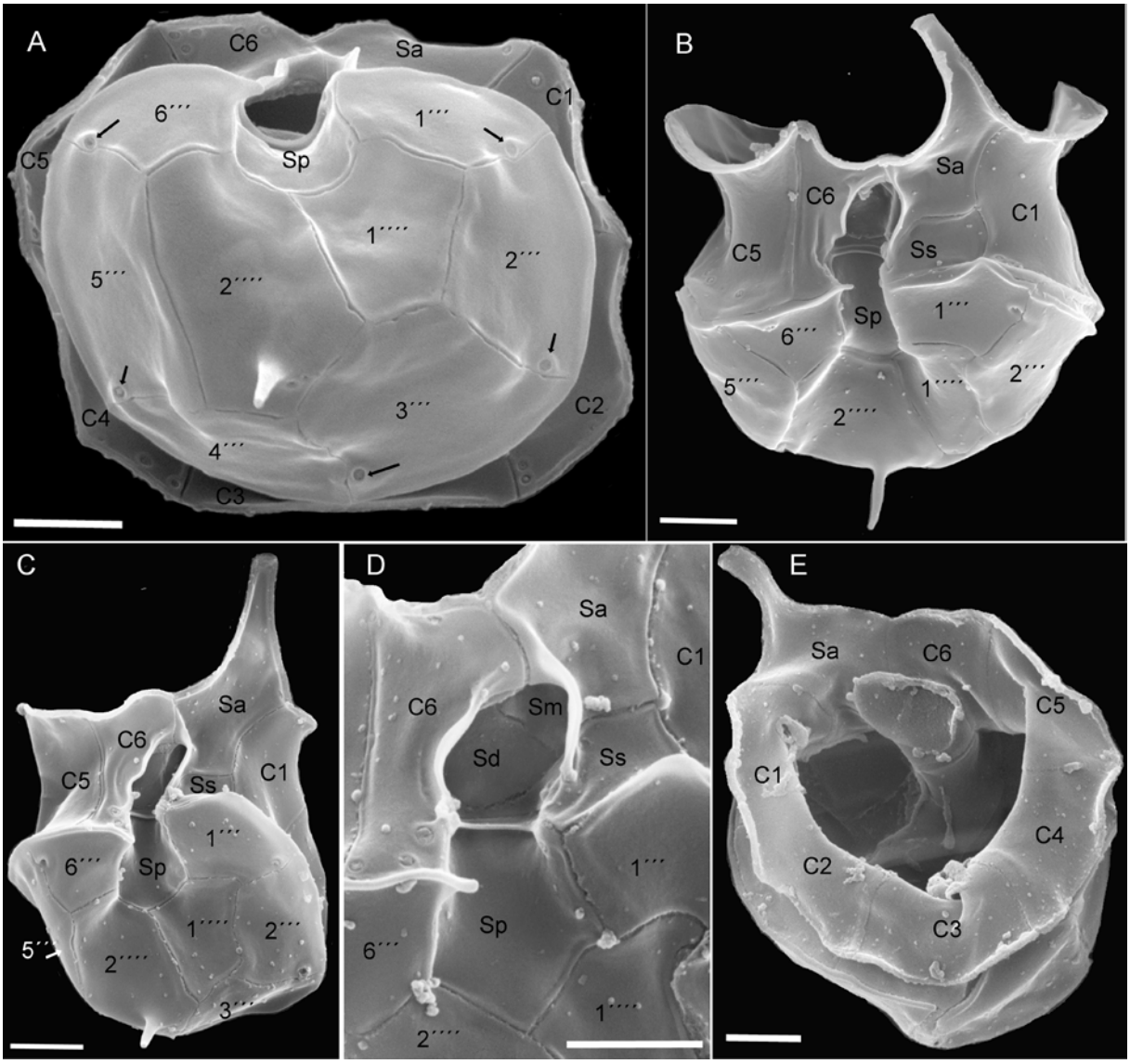
A
C6
Sa
C1
6‴
1‴
C5
Sp
1⁗
2‴
5‴
2⁗
C4
3‴
C2
4‴
C3
B
Sa
C6
C1
C5
Ss
Sp
1‴
6‴
5‴
1⁗
2‴
2⁗
C
Sa
C6
C5
Ss
C1
1‴
6‴
Sp
1⁗
2‴
5‴
2⁗
3‴
D
Sa
C1
C6
Sm
Sd
Ss
1‴
Sp
6‴
1⁗
2⁗
E
Sa
C6
C5
C1
C4
C2
C3

Fig. 17

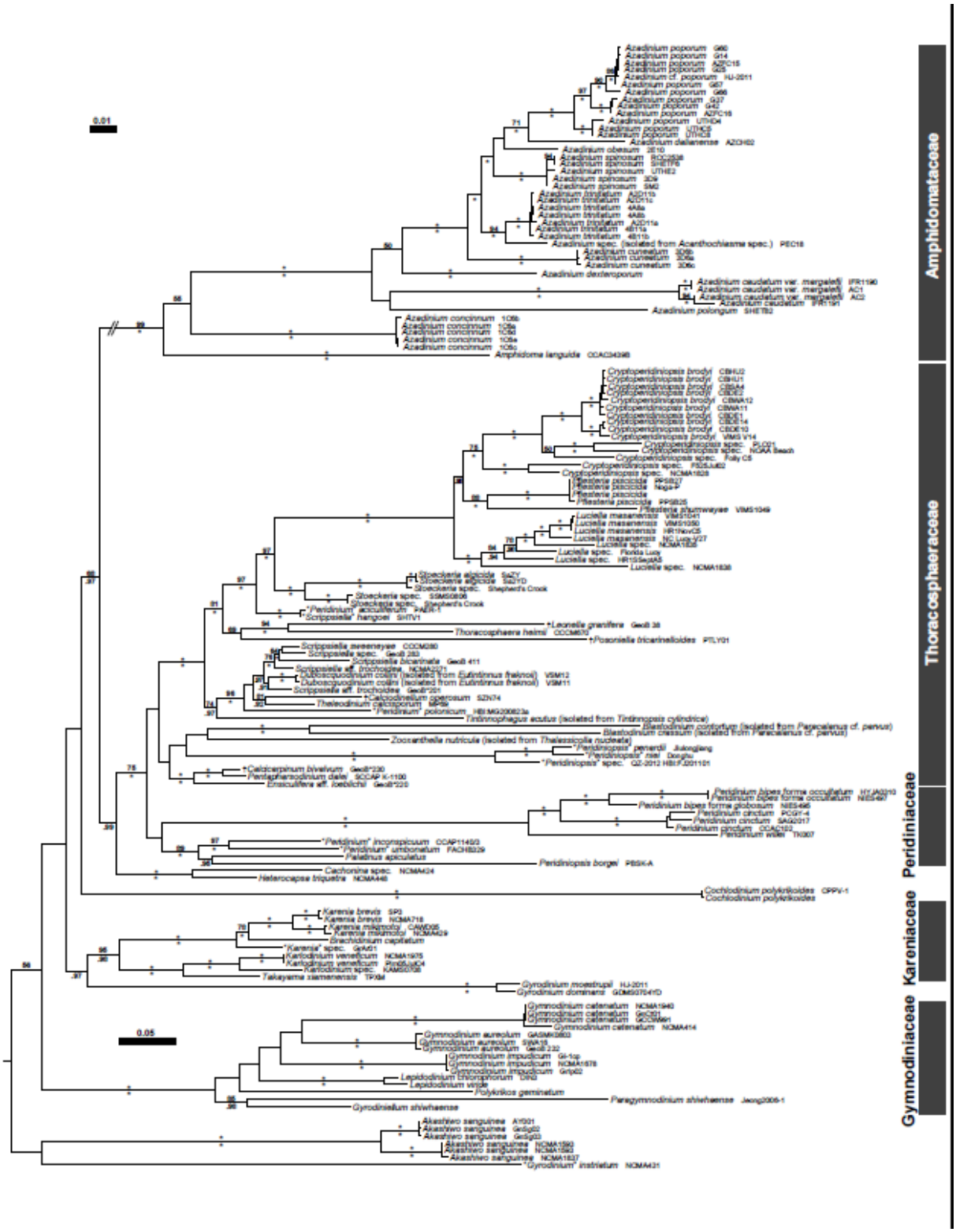
Amphidomataceae
Thoracosphaeraceae
Peridiniaceae
Kareniaceae
Gymnodiniaceae
0.01
0.05

Fig. 18

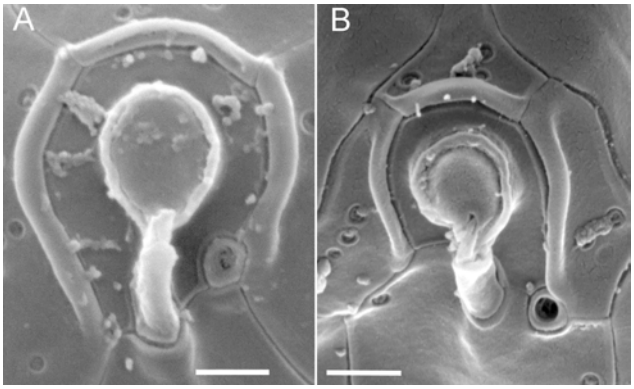

Fig. 19

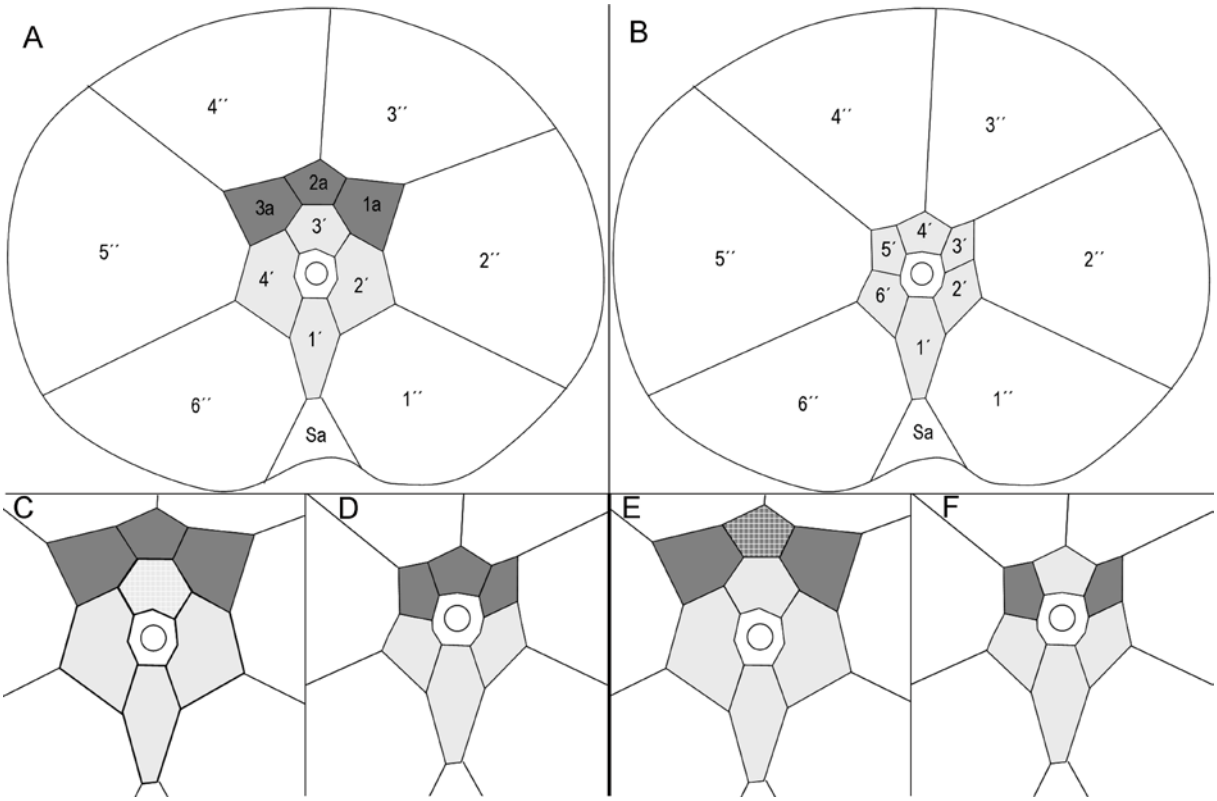

Fig. 20

Figure legend Supplementary material

Fig. S1: *Azadinium trinitatum*: Variations in plate pattern observed in cultivated cells. (A) Unusual contact of plate 2´ to plate 2a (white arrow). (B) Loss of contact between plate 3´ and 2a (white arrow). (C) Subdivision of plate 3a. (D) Subdivision of plate 4´. (E) Subdivision of both lateral apical plates 2´ and 4´. (F) Subdivision of plate 3´. (G) Subdivision of two plates on the apical right side (4´ and 5´´). (H) Subdivision of both plates 3´ and 2a. (I) Loss of the last intercalary plate 3a. Note that here plate 4´ unusually is in contact to 2a and that plate 4´´ is unusually small and triangular. (J) Antapical view showing the presence of just five postcingular plates (assumed to be the result of a fusion of plates 3´´´and 4´´´). (K) Antapical view showing the presence of just five postcingular plates (here assumed to be the result of a fusion of plates 2´´´and 3´´´). (L) Antapical view showing a reduction of both precingular and antapical plates. Scale bars = 2 µm.

Fig. S2: *Azadinium trinitatum*: Variations in plate pattern observed in culture. (A) A very rare case of plate 2a in penta-configuration (white arrow, plate 2a in contact to both plate 3´´ and plate 4´´). (B-C) Examples of cells with a particularly narrow posterior part of the first apical plate 1´ (white arrows). (D-G) Examples of cells with a rudimentary appearance of the antapical spine (white arrows). (H-I) Antapical view of cells without an antapical spine. (J-M) Compilation of all observed cases with a displaced ventral pore (white arrows). Scale bars = 2 µm.

Fig. S3: *Azadinium cuneatum*: Variations in plate pattern observed in culture. (A-B) Penta-configuration of plate 2a (i.e plate 2a is five sided and in contact to both plates 3´´ and 4´´). Note the asymmetric arrangement with the suture between plate 2a and 3´´ being

substantially longer than the suture between 2a and 4´´. (C) Plate 2a in a symmetric penta-configuration. (D-I) Examples of losses of one intercalary plate. Based on the absence of thecal pores the plate 2a was identified. (D-G) Loss of the first intercalary plate 1a. (H-I) Loss of the last intercalary plate 3a.

Fig. S4: *Azadinium cuneatum*: Variations of plate pattern observed in culture. (A) Reduction of each of the apical plate series to three apical, two intercalary, and five precingular plates. (B) Subdivision of both plate 4´ and 5´´. (C) Displacement of plate 3a getting in contact to the pore plate. (D) Fusion of plate 2´ and 3´. (E) Antapical view showing the presence of just five postcingular plates (here assumed to be the result of a fusion of plates 2´´´and 3´´´). (F-I) Compilation of all observed cases with a displaced ventral pore (white arrows). Scale bars = 2 µm.

Fig. S5: *Azadinium concinnum*: Variations of plate pattern observed in culture. (A-C) Loss of one epithecal intercalary plate. Note that either the first (A) or the last (B, C) intercalary has contact to three precingular plates. (D-E) Displacement of one intercalary plate to get in contact to the pore plate. (F) Detailed dorsal view of apical and intercalary plates indicating the loss of one intercalary plate. Note that the plate labelled here as 4´ might be a displaced intercalary plate 3a. (G) The first intercalary plate 1a displaced and in contact to the pore plate (white arrow). (H-I) Plate 3a displaced and in contact to the pore plate. (J) Loss of the middle intercalary plate 2a. Note that here plate 4´´ is small and without contact to an intercalary plate. (K) “Five” apical and two intercalary plates, here interpreted as a loss of plate 2a and a subdivision of plate 4´. (L) Loss of plate 2a and plate 3a displaced and in contact to the pore plate plate. (M) Antapical view showing the presence of just five postcingular plates (here assumed to be the result of a

fusion of plates 3´´´and 4´´´). Note the pore (white arrow) now disconnected to a plate suture. Scale bars = 2 µm (A, B, D, H, J-M) or = 1 µm (C, E-G, I).

Fig. S6: *Azadinium concinnum*: Variation of plate pattern observed in culture. (A-B) Loss of a single intercalary plate. Note that here plate 4´´ is small and not in contact to an intercalary plate. (C) Loss of a single intercalary plate. Note that here plate 5´´ is small and not in contact to an intercalary plate, (D-E) Loss of two intercalary plates. Note that in (E), there is also a fusion of plate 4´´ and 5´´. (F) Total loss of all intercalary plates. Note that plate 4´´ is small and the only precingular plate not in contact to an apical plate. (G) Loss of plates 3´ and 2a. (H) Loss of plate 3´, of two intercalary plates, and presence of just five precingular plates. (I) Detailed dorsal view of apical plates showing loss of plate 2a. (J-K) A “loss” of plate 2a most likely caused by a fusion of plates 3´and 2a. (L) Displacement of plate 2a not being in contact to the first intercalary plate 1a. (M) Loss of plate 2a. Scale bars = 2 µm (A-H, K-M) or = 1 µm (I, J).

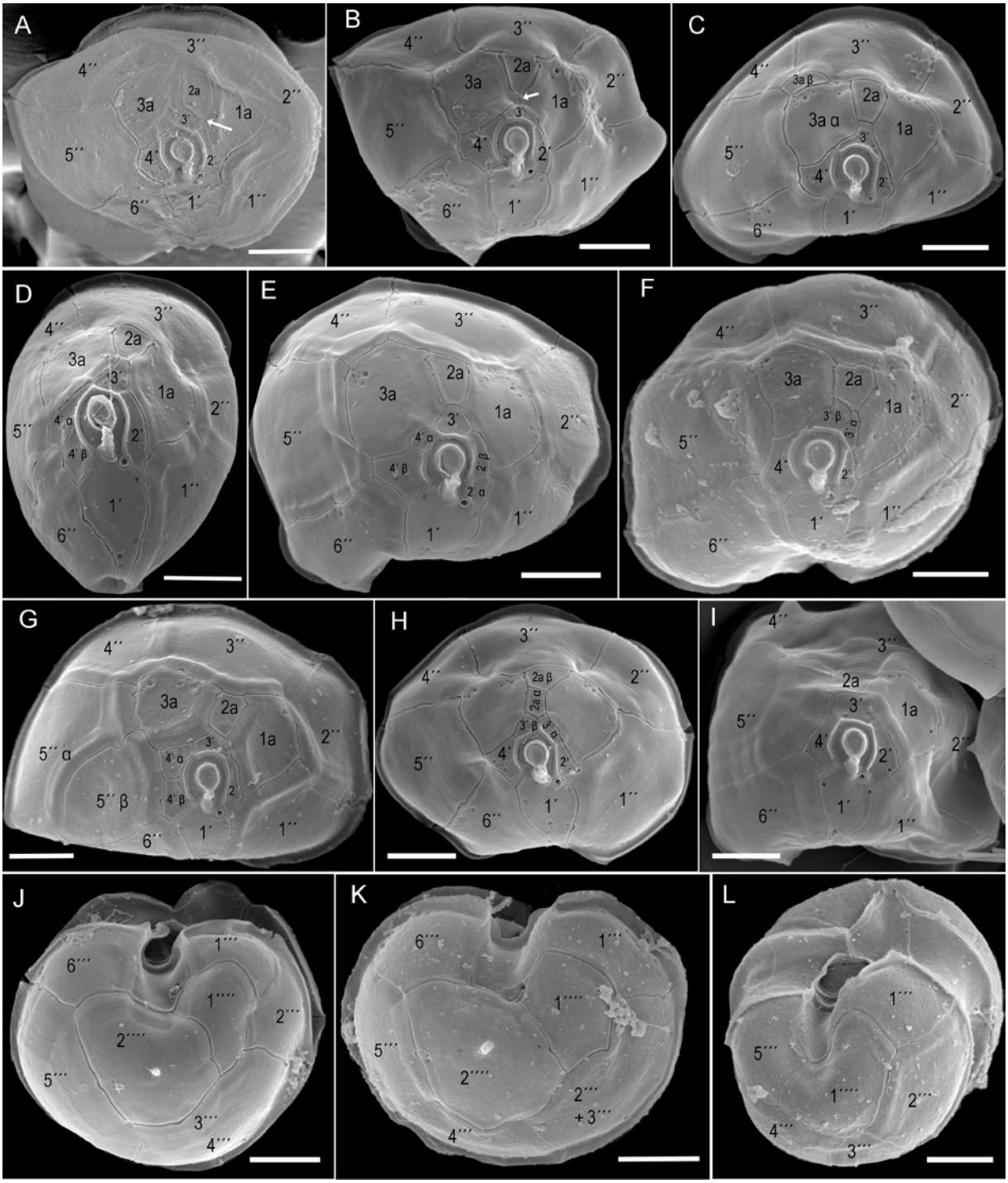

Suppl. Fig. S1

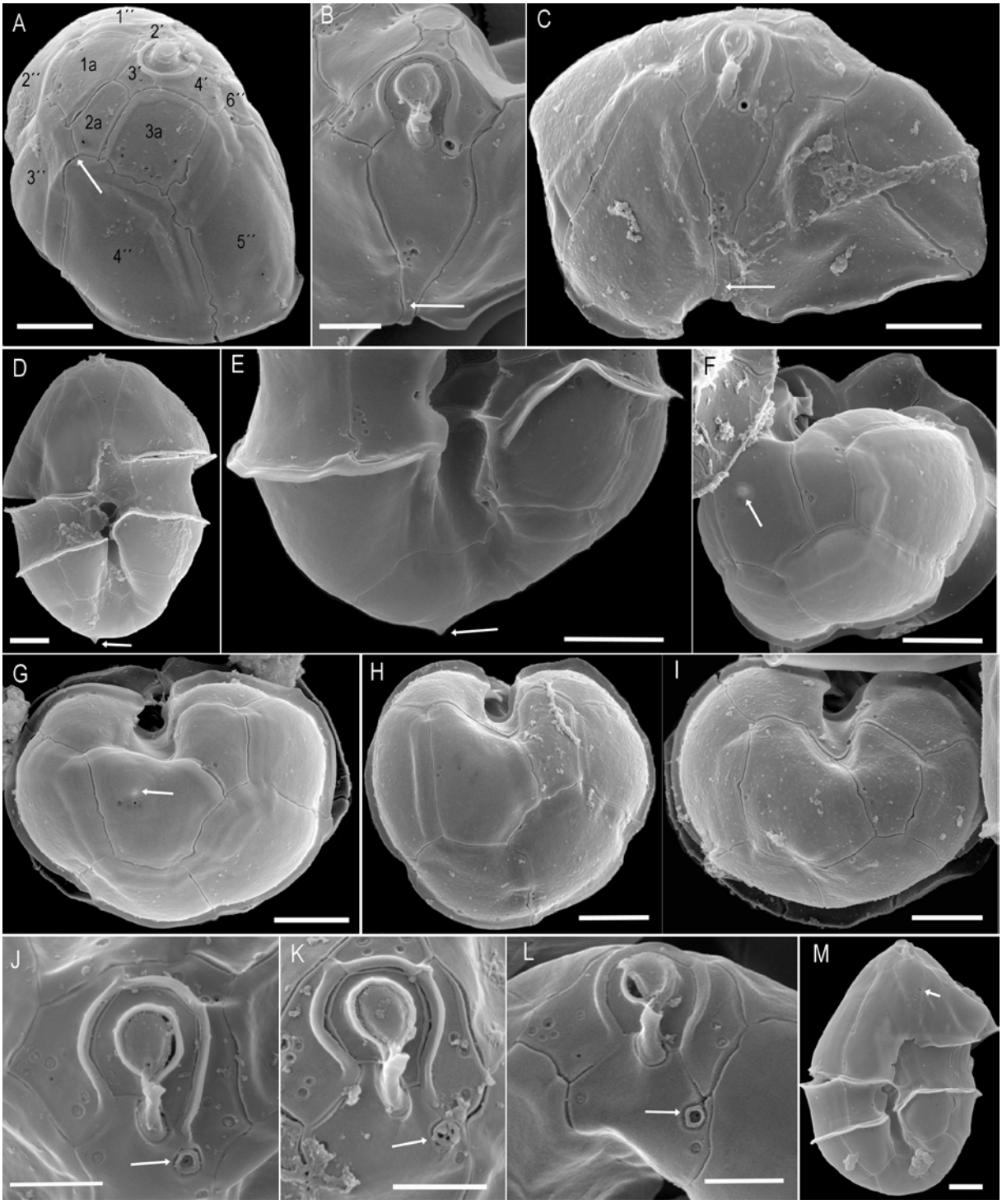

Suppl. Fig. S2

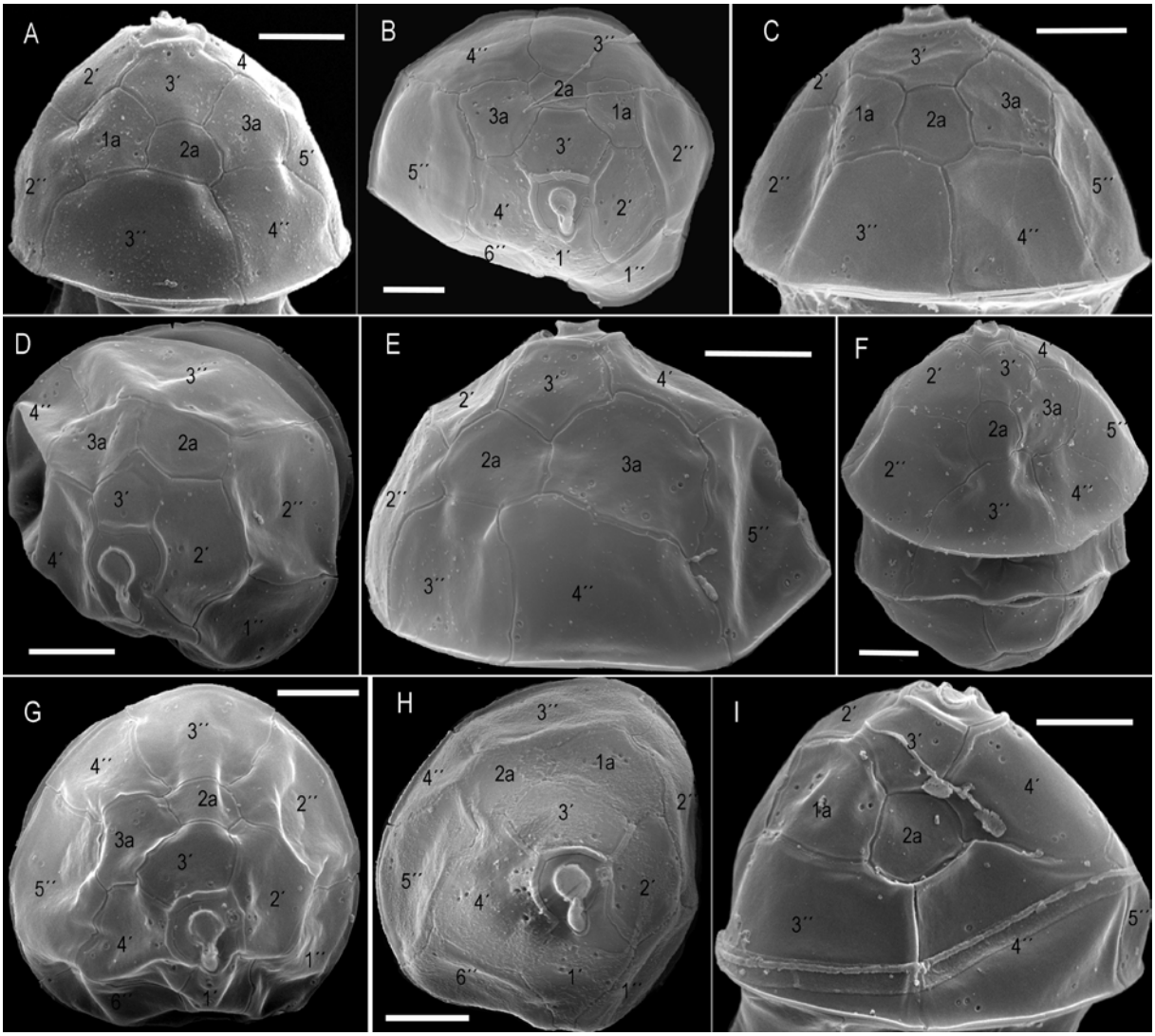

Suppl. Fig. S3

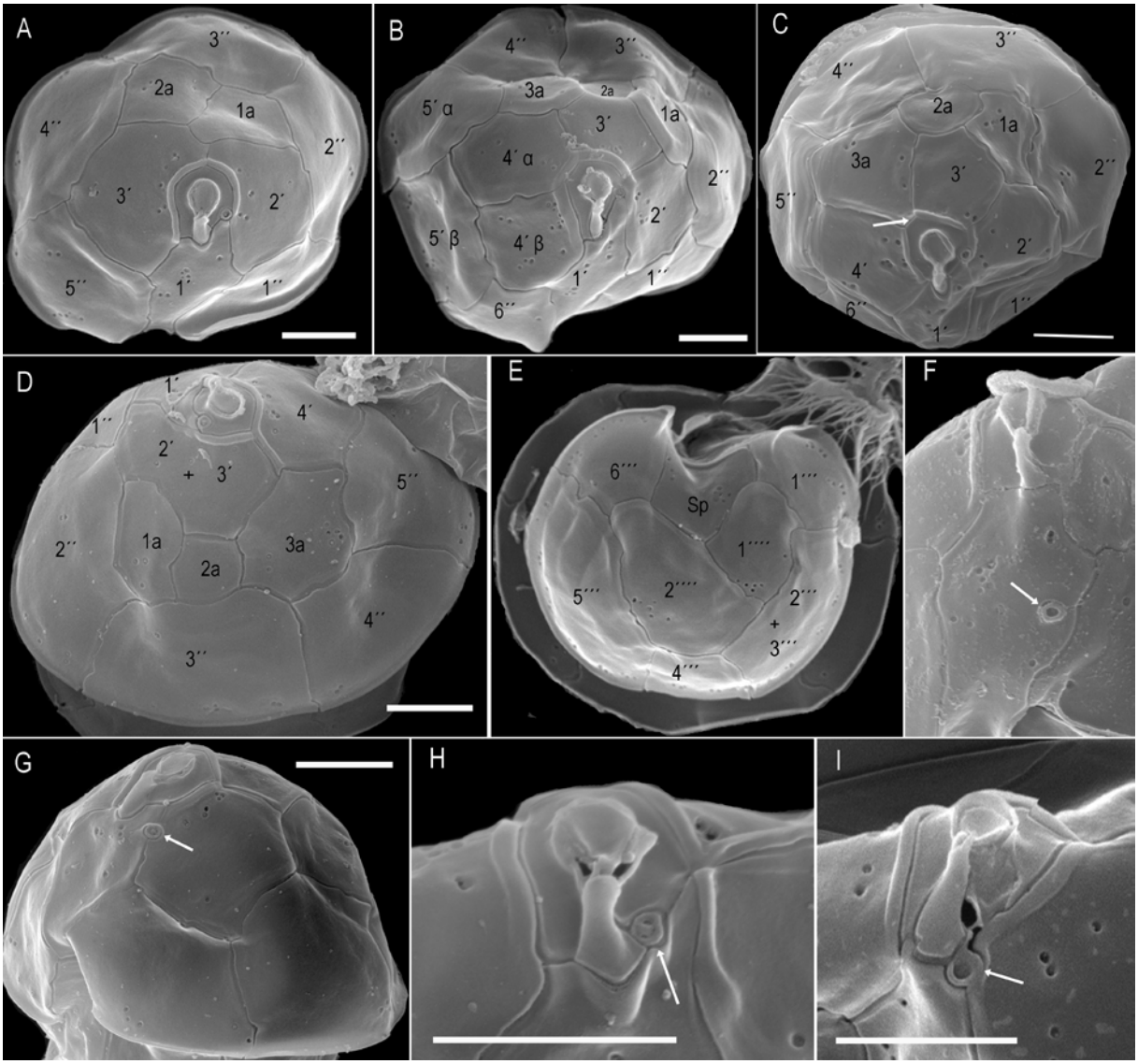
A
3´´
2a
1a
4´´
2´´
3´
2´
5´´
1´
1´´
B
4´´
3´´
3a
2a
5´ α
1a
3´
4´ α
2´´
2´
5´ β
4´ β
1´
1´´
6´´
C
3´´
4´´
2a
1a
3a
3´
2´´
5´´
2´
4´
6´´
1´´
1´
D
1´
1´´
4´
2´
+
3´
5´´
2´´
1a
3a
2a
4´´
3´´
E
6´´´
1´´´
Sp
1´´´´
5´´´
2´´´´
2´´´
+
3´´´
4´´´
F
G
H
I

Suppl. Fig. S4

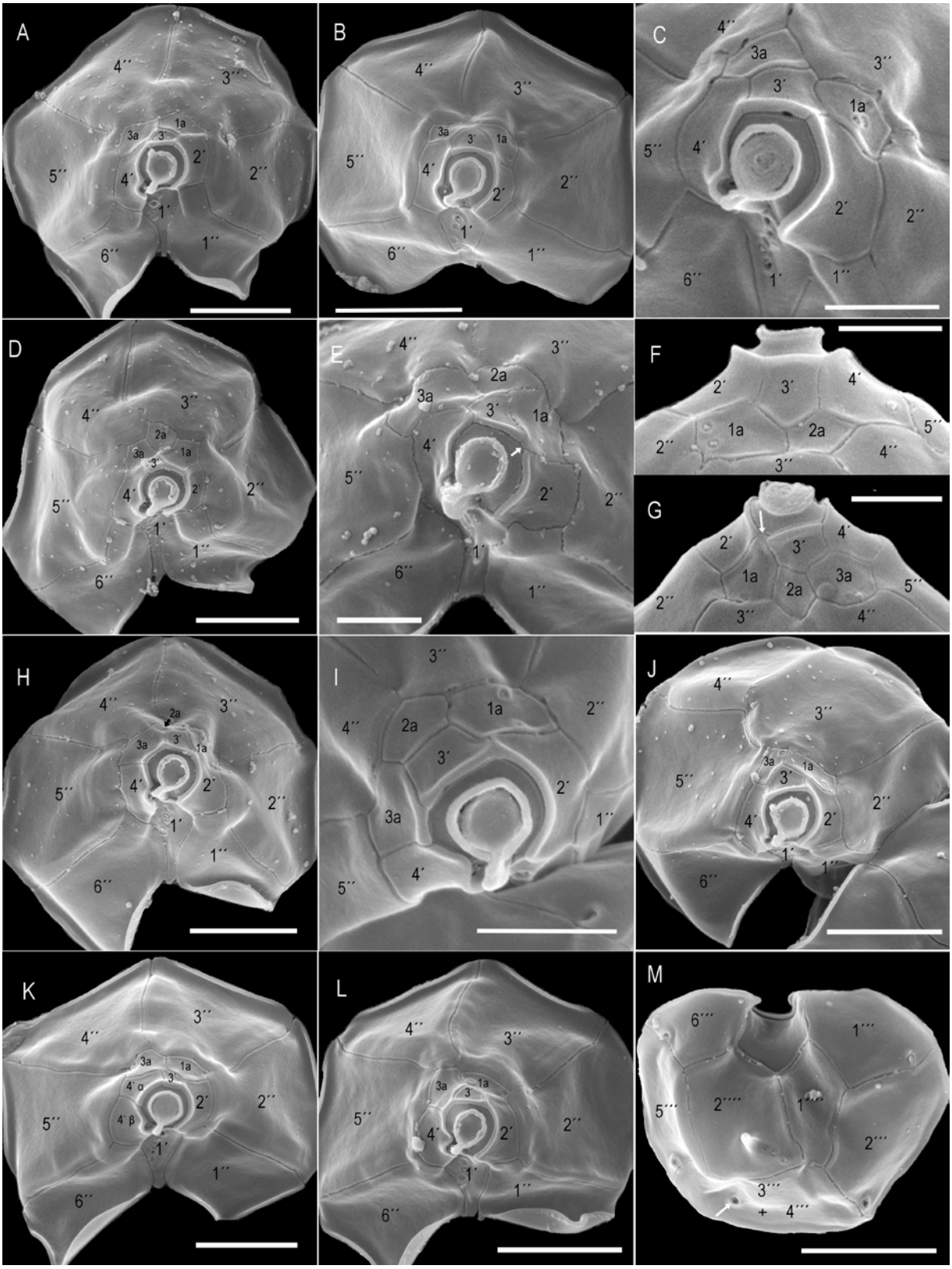

Suppl. Fig. S5

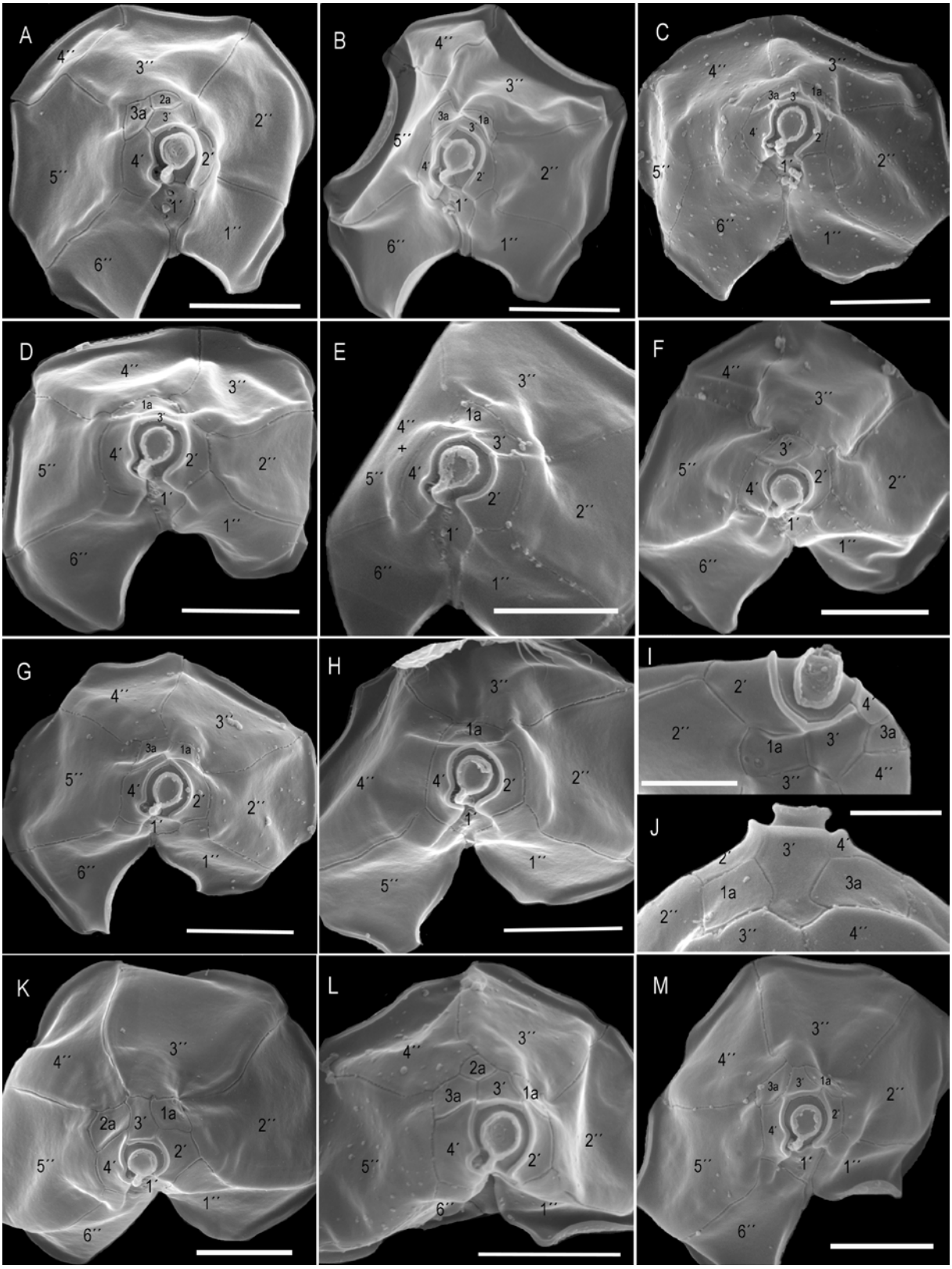

Suppl. Fig. S6